A new plesiosaurian from Jurassic-Cretaceous boundary of the Slottsmøya Member (Volgian), with insights into the cranial anatomy of cryptoclidids using Computed Tomography (#37185)

First submission

Guidance from your Editor

Please submit by **9 Jun 2019** for the benefit of the authors (and your $200 publishing discount).

Structure and Criteria
Please read the 'Structure and Criteria' page for general guidance.

Custom checks
Make sure you include the custom checks shown below, in your review.

Author notes
Have you read the author notes on the guidance page?

Raw data check
Review the raw data. Download from the location described by the author.

Image check
Check that figures and images have not been inappropriately manipulated.

Privacy reminder: If uploading an annotated PDF, remove identifiable information to remain anonymous.

Files

Download and review all files from the materials page.

34 Figure file(s)
5 Table file(s)
1 Video file(s)
1 Raw data file(s)
2 Other file(s)

Custom checks

Field study

- Have you checked the authors field study permits?
- Are the field study permits appropriate?

New species checks

- Have you checked our new species policies?
- Do you agree that it is a new species?
- Is it correctly described e.g. meets ICZN standard?

Structure and Criteria

Structure your review

The review form is divided into 5 sections. Please consider these when composing your review:

1. **BASIC REPORTING**
2. **EXPERIMENTAL DESIGN**
3. **VALIDITY OF THE FINDINGS**
4. General comments
5. Confidential notes to the editor

You can also annotate this PDF and upload it as part of your review

When ready submit online.

Editorial Criteria

Use these criteria points to structure your review. The full detailed editorial criteria is on your guidance page.

BASIC REPORTING

- Clear, unambiguous, professional English language used throughout.
- Intro & background to show context. Literature well referenced & relevant.
- Structure conforms to PeerJ standards, discipline norm, or improved for clarity.
- Figures are relevant, high quality, well labelled & described.
- Raw data supplied (see PeerJ policy).

EXPERIMENTAL DESIGN

- Original primary research within Scope of the journal.
- Research question well defined, relevant & meaningful. It is stated how the research fills an identified knowledge gap.
- Rigorous investigation performed to a high technical & ethical standard.
- Methods described with sufficient detail & information to replicate.

VALIDITY OF THE FINDINGS

- Impact and novelty not assessed. Negative/inconclusive results accepted. *Meaningful* replication encouraged where rationale & benefit to literature is clearly stated.
- All underlying data have been provided; they are robust, statistically sound, & controlled.
- Speculation is welcome, but should be identified as such.
- Conclusions are well stated, linked to original research question & limited to supporting results.

Standout reviewing tips

The best reviewers use these techniques

Tip	*Example*
Support criticisms with evidence from the text or from other sources	*Smith et al (J of Methodology, 2005, V3, pp 123) have shown that the analysis you use in Lines 241-250 is not the most appropriate for this situation. Please explain why you used this method.*
Give specific suggestions on how to improve the manuscript	*Your introduction needs more detail. I suggest that you improve the description at lines 57- 86 to provide more justification for your study (specifically, you should expand upon the knowledge gap being filled).*
Comment on language and grammar issues	*The English language should be improved to ensure that an international audience can clearly understand your text. Some examples where the language could be improved include lines 23, 77, 121, 128 – the current phrasing makes comprehension difficult.*
Organize by importance of the issues, and number your points	*1. Your most important issue* *2. The next most important item* *3. …* *4. The least important points*
Please provide constructive criticism, and avoid personal opinions	*I thank you for providing the raw data, however your supplemental files need more descriptive metadata identifiers to be useful to future readers. Although your results are compelling, the data analysis should be improved in the following ways: AA, BB, CC*
Comment on strengths (as well as weaknesses) of the manuscript	*I commend the authors for their extensive data set, compiled over many years of detailed fieldwork. In addition, the manuscript is clearly written in professional, unambiguous language. If there is a weakness, it is in the statistical analysis (as I have noted above) which should be improved upon before Acceptance.*

A new plesiosaurian from Jurassic-Cretaceous boundary of the Slottsmøya Member (Volgian), with insights into the cranial anatomy of cryptoclidids using Computed Tomography

Aubrey Jane Roberts [Corresp., 1, 2], **Patrick S Druckenmiller** [3, 4], **Benoit Cordonnier** [5], **Lene L Delsett** [6], **Jørn H Hurum** [6]

[1] Natural History Museum, London, United Kingdom

[2] National Oceanography Centre, University of Southampton, Southampton, United Kingdom

[3] University of Alaska Museum, Fairbanks, Alaska, United States

[4] Department of Geoscience, University of Alaska - Fairbanks, Fairbanks, Alaska, United States

[5] Institute of Geosciences, University of Oslo, Oslo, Norway

[6] Natural History Museum, University of Oslo, Oslo, Norway

Corresponding Author: Aubrey Jane Roberts
Email address: aubrey.roberts@nhm.ac.uk

Cryptoclidids are a major clade of plesiosauromorph plesiosaurians best known from the Middle – Late Jurassic, but little is known regarding their turnover into the Early Cretaceous. Of thirteen known cryptoclidid taxa, only five preserve cranial material and only one taxon has a complete, but compressed cranium. Thus, the lack of knowledge of the cranial anatomy of this group may hinder the understanding of phylogenetic intrarelationships, which are currently predominantly based on postcranial data. Here we present a nearly complete adult cryptoclidid specimen (PMO 224.248) representing a new taxon from the latest Jurassic – earliest Cretaceous part of the Slottsmøya Member, of central Spitsbergen. *Ophthalmothule cryosta* preserves a complete cranium, partial mandible, complete and articulated cervical, pectoral and anterior-mid dorsal vertebral series, along with the pectoral girdle and anterior propodials. High resolution micro computed tomography (µCT) ~~methods~~ were utilised to reveal new data on the cranial anatomy of this specimen. New internal features of the braincase and palate found using computed tomography~~,~~ were also confirmed present in other cryptoclidid specimens. Phylogenetic analysis including new characters, presents a new tree topology for the Cryptoclididae and particularly for the subfamily Colymbosaurinae. These results show that at least two cryptoclidid lineages were present in the Boreal Region during the Late Jurassic – Early Cretaceous and that representatives from these two lineages crossed the Jurassic – Cretaceous boundary at mid-high latitudes.

A new plesiosaurian from the Jurassic-Cretaceous boundary of the Slottsmøya Member (Volgian), with insights into the cranial anatomy of cryptoclidids using Computed Tomography

Authors: Aubrey J. Roberts [1,2], Patrick. S. Druckenmiller [3,4], Benoit Cordonnier [5], Lene L. Delsett [6] and Jørn H. Hurum[6]

[1]The National Oceanography Centre, University of Southampton, Southampton, Hampshire SO14 3ZH, United Kingdom

[2]The Natural History Museum, Exhibition Road, London, United Kingdom

[3]University of Alaska Museum, 907 Yukon Drive, Fairbanks, Alaska, 99775,

[4]Department of Geoscience, University of Alaska Fairbanks, 1962 Yukon Drive, Fairbanks, Alaska, 99775

[5]Physics of Geological Processes, Institute of Geosciences, University of Oslo, Norway

[6]The Natural History Museum, University of Oslo, Norway

Abstract

Cryptoclidids are a major clade of plesiosauromorph plesiosaurians best known from the Middle – Late Jurassic, but little is known regarding their turnover into the Early Cretaceous. Of thirteen known cryptoclidid taxa, only five preserve cranial material and only one taxon has a complete, but compressed cranium. Thus, the lack of knowledge of the cranial anatomy of this group may hinder the understanding of phylogenetic intrarelationships, which are currently predominantly based on postcranial data. Here we present a nearly complete adult cryptoclidid specimen (PMO 224.248) representing a new taxon from the latest Jurassic – earliest Cretaceous part of the Slottsmøya Member, of central Spitsbergen. *Ophthalmothule cryostea* preserves a complete cranium, partial mandible, complete and articulated cervical, pectoral and anterior-mid dorsal vertebral series, along with the pectoral girdle and anterior propodials. High resolution micro computed tomography (μCT) methods were utilised to reveal new data on the cranial anatomy of this specimen. New internal features of the braincase and palate found using computed

tomography, were also confirmed present in other cryptoclidid specimens. Phylogenetic analysis including new characters, presents a new tree topology for the Cryptoclididae and particularly for the subfamily Colymbosaurinae. These results show that at least two cryptoclidid lineages were present in the Boreal Region during the Late Jurassic – Early Cretaceous and that representatives from these two lineages crossed the Jurassic – Cretaceous boundary at mid-high latitudes.

Introduction

Plesiosauria is a clade of secondarily aquatic reptiles that predominantly inhabited marine environments during the Mesozoic Era. During the Jurassic, the plesiosaurian fossil record reveals a worldwide distribution and high level of morphological disparity (Benson, Evans and Druckenmiller, 2012). As with most other marine reptile groups, plesiosaur taxonomic diversity was heavily affected by eustatic sea-level changes during the Jurassic – Cretaceous transition (Tennant, Mannion and Upchurch, 2016), with the decline and replacement of some Jurassic clades by Xenopsaria (Benson and Druckenmiller, 2014). The Middle Jurassic – Early Cretaceous plesiosauroid family Cryptoclididae, is a species-rich clade primarily known from the Northern Hemisphere. The majority of the specimens derive from the Oxford and Kimmeridge Clay Formations of the UK. The recent recovery and description of numerous cryptoclidid specimens from the Slottsmøya Member Lagerstätte of the Agardhfjellet Formation (central Spitsbergen), now constitute a major component of overall Boreal plesiosaurian richness from the Tithonian-Berriasian interval (Druckenmiller et al., 2012;

Cryptoclididae includes the subclade Colymbosaurinae [Benson and Bowdler, 2014] and another clade yet to be formally named. ~~The~~ Colymbosaurinae~~,~~ previously included all the described plesiosauroid taxa from the Slottsmøya Member (*Djupedalia engeri*, *Spitrasaurus wensaasi*, *S. larseni*, *Colymbosaurus svalbardensis*), in addition to *Abyssosaurus nataliae*, *Pantosaurus striatus* and *Colymbosaurus megadeirus* (Benson and Bowdler, 2014). As noted by Benson and Bowdler (2014), the cranial anatomy of cryptoclidids is poorly known and thus the diagnosis of Colymbosaurinae is based exclusively on postcranial characters. The new specimen described here, PMO 224.248, is significant in that it preserves a complete cranium and partial postcranium representing a new genus of cryptoclidid plesiosaur, *Ophthalmothule cryostea*. PMO 224.248 was excavated in 2012 out the Slottsmøya Member of the Agardhfjellet Formation, from a part of the unit section encompassing the Jurassic – Cretaceous boundary. The specimen

represents the fourth and youngest cryptoclidid described from the Slottsmøya Member and based on micro Computed Tomography (μCT) imaging, adds significant new data on the cranial anatomy of cryptoclidids and plesiosaurians in general. These data contribute to a revised phylogenetic hypothesis of cryptoclidid phylogeny and shed light on turnover at the Jurassic - Cretaceous boundary.

Geological Setting

The Agardhfjellet Formation encompasses a thick succession of Middle Jurassic to Lower Cretaceous sedimentary rocks. The formation comprises four members; Oppdalen Member, Lardyfjellet Member, Oppdalsåta Member and the Slottsmøya Member. The Slottsmøya Member (Volgian) consists of dark-grey to black silty mudstone, which is often weathered into paper shale. There are discontinuous silty beds, with siderite concretions, in addition to siderite and dolomite interbeds. The Slottsmøya Member is overlain by the Lower Cretaceous Myklegardfjellet Bed, which defines the base of the Rurikfjellet Formation (Fig. 1A; Dypvik et al., 1991).

The Slottsmøya Member was deposited in an open marine environment under dysoxic conditions (Collignon and Hammer, 2012). These marine deposits represent approximately 12 million years of deposition from the upper Tithonian (uppermost Jurassic) to the lower Berriasian (lowermost Cretaceous; Hammer, Collignon and Nakrem, 2012). The member is divided into three units; a lower (-22-0m), middle (0-27m) and an upper unit (27-52? m) (Collignon and Hammer, 2012). The specimen (PMO 224.248) described here derives from the upper unit (at 38.5 m), which is increasingly condensed up section, making it difficult to precisely determine if this specimen derives from the uppermost Jurassic or lowermost Cretaceous (Fig. 1B). However, the seeps overlying the specimen in the stratigraphy are determined to be from the Early Cretaceous (Hryniewicz et al., 2012).

Materials and Methods

Measurements

Measurements were taken using a calliper or tape measure for longer measurements (>15 cm), these are available in the supplementary information (Tables S.1-4). For some of the braincase

elements that were obscured by matrix or another element, measurements were taken using the µCT scan images.

µCT methodology

The cranium, left mandible, eighth cervical vertebra and possible gut contents were scanned using µ-Computer Tomography (µCT) and the University of Oslo Natural History Museum (Økern Campus). Figures of the volume renderings of the complete posterior of the skull, lower jaw and 8th cervical vertebra are shown in the supplementary materials (Figs. S.2, S.6). Due to the size limitations of the scanner, three separate scans of the cranium (posterior, middle and anterior of the cranium), were taken and then merged together to form a single high-resolution scan. For the cranium: a total volume of 7 274 887 cm^3 was acquired using a Nikon XT H 225 ST desktop CT scanner, with a spatial resolution equal to a voxel size of 0.0753767 mm^3. A 2mm copper filter was utilised. For each scan, tomographic acquisition was performed under step rotation with an exposure time of 2000 ms, the beam energy was 180 keV and 3016 projections were taken over 360º. For the left mandible, two CT scans were performed and then merged, using the same settings as for the cranium. These consisted of 1583 projections taken over 360°, with an exposure time of 1000 ms. The 8th cervical vertebra was scanned with 3016 projections taken over 360°, with 1000 ms exposure, with the same settings as for the cranium.

Manual segmentation of the braincase was performed with the 3D analysis software Aviso Fire (V. 8.1) and Fiji (ImageJ) at the University of Southampton µ-vis (Muvis) Digital Visualisation Laboratory. The automatic segmentation of the complete cranium was pre-processed with a growing algorithm developed by CB in MATLAB (V. 2016b). This eliminated some of the surrounding and internal matrix from the volume rendering using differences in density. A video of the complete volume rendered skull is available in the supplementary information. The complete raw data is available for download from Morphosaurce.org (P774).

Permits

The following permits were given by the Governor of Svalbard for the University of Oslo Natural History Museum excavations in 2007, 2010, 2011 and 2012: 2006/00528-13; RIS ID 3707; RIS ID: 4760 and 2006/00528-39.

Institutional abbreviations

CAMSM, Cambridge Sedgewick Museum, Cambridge, United Kingdom; **NHMUK**, Natural History Museum, London, United Kingdom; **MGUH**, Geological Museum, Copenhagen, Denmark; **PETMG**, Peterborough Museum and Art Gallery, United Kingdom; **PMO**, Palaeontology museum, Natural History Museum, Oslo, Norway; **OUM**, Oxford University Museum, United Kingdom; **SVB**, Svalbard Museum, Norway; **UW**, University of Wyoming, Wyoming, United States of America.

Nomenclatural acts

The electronic version of this article in Portable Document Format (PDF) will represent a published work according to the International Commission on Zoological Nomenclature (ICZN), and hence the new names contained in the electronic version are effectively published under that Code from the electronic edition alone. This published work and the nomenclatural acts it contains have been registered in ZooBank, the online registration system for the ICZN. The ZooBank LSIDs (Life Science Identifiers) can be resolved and the associated information viewed through any standard web browser by appending the LSID to the prefix http://zoobank.org/. The LSID for this publication is: [LSID urn:lsid:zoobank.org:pub:3578E578-4724-45FE-8CEE-C075D5C54F34]. The online version of this work is archived and available from the following digital repositories: PeerJ, PubMed Central and CLOCKSS.

Systematic Palaeontology

Sauropterygia Owen, 1860

Plesiosauria de Blainville, 1835

Plesiosauroidea Welles, 1934

Cryptoclididae Williston, 1925

Ophthalmothule genus nov.

LSID urn:lsid:zoobank.org:act:63110850-0CAC-4DBA-99C2-7AC3B6B926DB

Diagnosis as for the species

Ophthalmothule cryostea sp. nov

LSID urn:lsid:zoobank.org:act:97CEBF5F-58FE-472F-AFA4-9C00E37BB834

(Figures 2 – 19)

Holotype: PMO 224.248

Occurrence: The holotype specimen PMO 224.248 was excavated from the north-facing slopes of Wimanfjellet (Mt. Wiman), from the upper part of the Slottsmøya Member, Agardhfjellet Formation, central Spitsbergen: GPS coordinates UTM 33X E523620 N8696396 (Fig. 1). The specimen was located 38.5 m above the yellow storm deposit marker bed (0m in log), and is late Volgian (latest Tithonian/ early Berriasian) in age.

Etymology: *Ophthalmothule*. *Ophthalmo*, meaning eye. *Thule* is a term used for the northern-most region of the world. Together they make "North eye". Species name, *cryostea*, meaning "frozen bones".

Differential diagnosis

A moderately sized cryptoclidid plesiosaur (estimated body length of 5.0-5.5 m), possessing the following autapomorphies unique among Cryptoclididae (*) and unique character combinations: premaxilla bears 6 alveoli (5 in *Tricleidus seeleyi* and *Muraenosaurus leedsii*); medial margin of premaxilla terminates anterior to the posterior margin of external naris (*); maxilla bears an estimated 16 alveoli (18 in *Cryptoclidus eurymerus*; 15 in *Tricleidus seeleyi*); frontal twice as anteroposteriorly long as parietal (subequal or shorter in *Cryptoclidus eurymerus* and *Muraenosaurus leedsii*); frontal participates in the medial and posterior margins of the external naris (participates posteriorly in *Muraenosaurus leedsii*); presence of an interfrontal vacuity (absent in *Muraenosaurus leedsii*); dorsoventrally low but narrow sagittal crest (flat and broad in *Kimmerosaurus*); quadrate articulates anterolaterally to the pterygoid (posteromedially in *Tricleidus seeleyi* and *Muraenosaurus leedsii*); lateral cotyle of quadrate larger than medial cotyle (reversed in *Spitrasaurus larseni*); basioccipital tubera broad and flattened (circular in *Kimmerosaurus langhami* and *Cryptoclidus eurymerus*); basioccipital tubera triangular in ventral view, following the anteromedial process of pterygoid anteriorly (cylindrical with finished bone anteriorly in *Kimmerosaurus langhami*); exoccipital does not contribute to occipital condyle

(contributes in *Kimmerosaurus langhami* and *Cryptoclidus eurymerus*); posteromedian ridge on supraoccipital absent (present in *Kimmerosaurus langhami* and *Muraenosaurus leedsii*); palatine and vomer excludes maxilla from internal naris (maxilla participates in *Muraenosaurus leedsii*); vomer excluded from anterior interpterygoid vacuity (participates in *Muraenosaurus leedsii* and *Cryptoclidus eurymerus*); anteromedial process of pterygoid extends as far as the parabasisphenoid (absent in *Cryptoclidus eurymerus*); dentary with a mediolaterally extended alveolar surface and with laterally shifted, labially inclined alveoli (no mediolateral extension and alveoli positioned centrally in *Tricleidus*); deep glenoid facet of the mandible, constituting over half the dorsoventral height of the mandible (relatively shallow in *Colymbosaurus* spp., *Cryptoclidus eurymerus* and *Kimmerosaurus langhami*); retroarticular process slightly dorsally inclined (significantly inclined in *Spitrasaurus larseni*); faint longitudinal ridged teeth, distinct on labial side (distinct on lingual side in *Muraenosaurus leedsii* and *Cryptoclidus eurymerus*; ridging absent in *Kimmerosaurus langhami*); slightly recurved tooth crowns (significantly recurved in *Spitrasaurus larseni* and *Kimmerosaurus langhami*); hypophyseal eminence present on ventral surface of atlas (ventral keel in *Cryptoclidus eurymerus*, *Muraenosaurus leedsii* and *Tricleidus seeleyi*); atlantal rib present (absent in *Colymbosaurus megadeirus*); 50 cervical vertebrae* (32 in *Cryptoclidus eurymerus*; 44 in *Muraenosaurus leedsii*; 41 in *Colymbosaurus megadeirus*; 60 in *Spitrasaurus wensaasi*); cervical centra are slightly amphicoelous (conspicuously concave in *Djupedalia engeri* and *Kimmerosaurus langhami*); cervical vertebra 8 with anteroposteriorly long postzygapophyses, close to the length of centrum (autapomorphic among Plesiosauria); anterior-most cervical neural spines low and posteriorly angled (straight in *Kimmerosaurus langhami*); cervical prezygapophyses unfused anteriorly and fused posteriorly (unfused throughout in *Cryptoclidus eurymerus* and completely fused in *Spitrasaurus* spp. and *Djupedalia engeri*); postzygapophyses fused along the midline (unfused in posterior-most cervicals in *Djupedalia engeri*); lateral ridges present on mid-posterior cervicals (absent in *Colymbosaurus megadeirus*, *Cryptoclidus eurymerus*, *Djupedalia engeri*, *Kimmerosaurus langhami* and *Tricleidus seeleyi*); posterior cervical – anterior dorsal ribs with a distinct longitudinal ridge*; dorsal vertebral rib facets dorsoventrally taller than wide (circular in *Tatenectes laramiensis*); dorsal process of scapula short and reduced (tall and extensive in *Abyssosaurus nataliae* and *Djupedalia engeri*); extended anteromedial process of coracoid (reduced in *Colymbosaurus megadeirus* and *Abyssosaurus nataliae*); humeri significantly larger than femora (femora larger than humeri in *Djupedalia engeri*,

subequal in *Colymbosaurus svalbardensis*); sigmoid humerus in dorsal view*; forelimbs with three to four distal articular facets (two in *Cryptoclidus eurymerus* and *Muraenosaurus leedsii*); radius slightly larger than ulna (anteroposteriorly shorter in *Colymbosaurus svalbardensis*).

Taphonomy

The near-complete skeleton of PMO 224.248 is well-preserved and fully articulated, with the exception of the skull, some dorsal vertebrae and distal phalangeal elements (Fig. 2). The skeleton had a ventral landing and the cranium drifted 20 cm from its original position, and the majority of the phalanges drifted from the limbs and were not preserved in articulation. The skeleton posterior of the sacral region was eroded, although a partial left hindlimb and femoral fragments were recovered.

The specimen preserves a complete skull, although it is dorsoventrally crushed and damaged in places. The cranium could not be completely prepared from the matrix, as the bones where significantly fractured. The dorsal portions of the braincase were partly disarticulated due to the crushing, with the supraoccipital pushed down into the foramen magnum. The majority of the cervical vertebrae are missing portions of the right cervical rib and neural spines, due to crushing and/or pre-burial erosion. The posterior-most cervicals were disarticulated and crushed by the overlying pectoral girdle. The pectoral and anterior dorsal vertebrae are partly crushed and distorted by the overlying pectoral girdle. Most of the neural arches are missing from the dorsal vertebrae, as these were exposed to post-diagenetic erosional processes.

Ontogeny

PMO 214.248 is interpreted to be an adult based on its large size and presence of fused neurocentral sutures throughout the preserved vertebral column, in addition to the fusion of the cervical ribs to the centra (Brown, 1981). Other indicators of mature stage of are the fusion along the medial facet of the coracoids and well-formed distal facets of the humeri (Brown, 1981).

Description and comparison with other cryptoclidid taxa

Cranium

The temporal fenestrae are conspicuously small relative to the size of the orbits, being approximately 17 % of total skull length, whereas the orbit constitutes approximately 29 % of total

skull length (Figs. 3-5). The tooth row extends about 75 % of the total skull length. For selected measurements of the cranium see supplementary information (Table S1).

Premaxilla

The premaxilla of *Ophthalmothule cryostea* forms the majority of the dorsal and lateral surfaces of the rostrum anterior to the orbit (Fig. 3.3). As with all cryptoclidids (at least those few that preserve cranial material), the rostrum is relatively short (Andrews, 1910; Brown and Cruickshank, 1994), having a preorbital to total skull length ratio of 0.43. Although this appears high in comparison to other cryptoclidids, it is due to relatively short post orbital region of the skull. Similar to *Muraenosaurus leedsii*, the dorsal surface of the premaxilla is rugose, forming numerous low and sharp crests (Andrews, 1910). The premaxillae form a narrow ridge that extends along most of the rostral midline. The anterior portion of the premaxilla-maxilla suture is visible in dorsal view, extending from the rostral margin towards the external naris. The external nares of *Ophthalmothule cryostea* are positioned immediately anterior to the orbital margin, being relatively more posterodorsally placed than in *M. leedsii*. In *O. cryostea*, the dorsomedial process of the premaxilla, forms the anterior and anteromedial borders of the external naris. However, the process terminates anterior to the posteromedial margin of the external naris, representing an autapomorphy of this taxon among cryptoclidids. In *Cryptoclidus eurymerus* the morphology of this region is ambiguous (in PETMG R.283.412); however, it has been reconstructed with the premaxillae excluded from most of the medial margin of the external naris by the frontal (PETMG R.283.412; Brown and Cruickshank, 1994). This morphology is not homologous with the condition where the anterior flange of the frontal, excludes the premaxilla from the external naris as in some rhomaleosaurids (Smith and Benson, 2014). In *M. leedsii* and *Tricleidus seeleyi*, the premaxillae form the medial margin of the external nares and either terminate at or continue past the posterior margin of the external nares (Andrews 1910; Brown, 1981). The µCT scans of PMO 224.248 confirm that the premaxilla overlaps the anterior portion of the frontal and that this sutural contact lies approximately in line with the external naris, as in *C. eurymerus* (PETMG R.283.412; Andrews, 1910; Brown and Cruickshank, 1994). Furthermore, in *Ophthalmothule cryostea* the premaxilla-frontal suture is embayed anteriorly along the midline with the longest dimension of the premaxilla occurring in the parasagittal plane. In contrast, the dorsomedial process of the premaxilla taper posteriorly along the midline in *C. eurymerus* and *M. leedsii*.

Among cryptoclidids the number of premaxillary alveoli varies between 5-8 teeth on each side (Brown, 1981). Based on µCT data (Fig. 4B), the premaxilla of *Ophthalmothule cryostea* has a total of six alveoli on each side, the same number as *Cryptoclidus eurymerus* (Brown and Cruickshank, 1994), but greater than that observed in *Muraenosaurus leedsii* (five: Brown, 1981) and less than that suggested for *Kimmerosaurus langhami* (minimum eight: Brown, 1981). The first and sixth alveoli are noticeably smaller in all dimensions than the other premaxillary alveoli, which are otherwise similar in size. The premaxillary-maxillary suture is visible in ventral view, just posterior to the sixth alveolus (Figs. 4-5).

Maxilla

The maxilla of *Ophthalmothule cryostea* forms the ventral rim and most of the anterior margin of the orbit. In dorsal view, the prefrontal-maxilla suture is equivocal due to significant breakage in this region. The lateral surface of the maxilla is lightly pitted and rugose, but not to the same extent as the premaxilla. In ventral view the alveoli are partially obscured by matrix, but can be counted using µCT images, showing a maximum of 16 alveoli on both sides when taking damage into account. This is less than *Cryptoclidus eurymerus* (18; Brown, 1981), but similar to other Oxford Clay Formation cryptoclidids (16 in *Muraenosaurus leedsii*; 15 in *Tricleidus seeleyi*; Brown, 1981). The maxillary alveoli vary only slightly in size and morphology, with the larger labiolingually expanded alveoli located more anteriorly and smaller, more rounded alveoli posteriorly. We interpret that the slight asymmetry regarding maxillary alveolus size present in *Ophthalmothule cryostea* is likely due to variation in tooth replacement stage. This morphology differs from *T. seeleyi*, where clear heterodonty is present (Brown, 1981). As in *C. eurymerus* (PETMG R.283.412), the posterior extent of the maxillary tooth row in *Ophthalmothule cryostea* terminates in line with the position of the postorbital bar and is positioned considerably higher than the glenoid fossa in lateral view.

Ventrally, the maxilla approaches and nearly contributes to the margin of the internal naris, but is excluded by the palatine-vomer contact, similar to *Cryptoclidus eurymerus* (Andrews, 1910). This morphology differs from *Muraenosaurus leedsii* where the premaxilla and maxilla contribute to the anterior and lateral margins of the internal naris respectively (Andrews, 1910; Brown and Cruickshank, 1994).

Prefrontal

The region anterior to the orbit in PMO 224.248 is difficult to interpret, due to poor preservation. There are two possible sutures that could represent the lateral and medial margins of a prefrontal, with the position of these sutures confirmed by differences in bone orientation using µCT images (Supplementary Information, Fig. S.1). Using these margins, the prefrontal would be constrained to a small wedge-shaped section directly anterior to the orbital rim, separated from the external naris by a dorsal process of the maxilla. The element is thickened along the orbital margin and posterodorsally overlaps the frontal in a pointed process. The prefrontal is rarely described in Callovian cryptoclidids, with the exception of *Muraenosaurus leedsii* (Andrews, 1910; Brown, 1981). This has been attributed to either poor preservation of this area in most specimens, or because the element is indiscernible due to fusion with the maxilla (Brown, 1981; *pers. obs.* PSD).

Frontal

In *Ophthalmothule cryostea*, the anteroposterior length (measured along the midline) of the frontal is 2.3 times longer than the length of the parietal, whereas in other taxa the relative lengths are nearly the same (= ~0.9 *Cryptoclidus eurymerus* PETMG R.283.41; = ~1 *Cryptoclidus eurymerus* NHMUK R2860; = ~0.8 *Muraenosaurus leedsii* using Andrews, 1910; = ~1.4 *Tricleidus seeleyi* NHMUK R3539). Anteriorly, the frontal participates in the medial and posterior margins of the external naris. In *M. leedsii*, the frontal participates in the margin of the external naris, but lacks the same degree of anterior extension seen in *Ophthalmothule cryostea* (Andrews, 1910). As in *M. leedsii*, the greatest mediolateral width of the frontal occurs directly in line with the anterior margin of the orbit, in contrast to *C. eurymerus* where this occurs more posteriorly along the middle orbital margin (Andrews, 1910; Brown and Cruickshank, 1994). At the point of articulation with the parietal the mediolateral width of the element is roughly a third of the maximum mediolateral width. Along the dorsal margin of the orbit, the frontal has a concave margin, differing considerably from the straight frontal margin of *Muraenosaurus* specimens (*M. leedsii*; NHMUK R.2678) and from *C. eurymerus,* where it is convex (*C. eurymerus*; PETMG R.283.412). The relationships of the postfrontal and postorbital to the skull roof are not preserved.

The frontals vary in the degree to which they contact one another along the dorsal midline. At their anterior- and posterior-most ends (adjoining the premaxillary and parietal contacts, respectively), the frontals are fully in contact and fused along the midline. However, along the remainder of their length they lack a firm midline contact and enclose a narrow and elongate slit-

like opening, referred to here as the interfrontal vacuity. This vacuity is not homologous to the "frontal foramen" observed near the anterior margin of the frontal in some polycotylids, which is not located along the midline (Carpenter, 1996). However, this vacuity ~~does bear some resemblance to~~ the dorsomedian frontal foramen described in *Brancasaurus brancai* (Sachs, Hornung and Kear, 2016). The most conspicuous development of the interfrontal vacuity occurs in the anterior half of the frontals where it can be recognised by having smooth, finished bone medially and a slight concavity following the midline. An interfrontal vacuity is also clearly present in several other cryptoclidids (e.g. *Kimmerosaurus langhami*; *Tatenectes laramiensis*; *Tricleidus seeleyi*; possibly *Cryptoclidus eurymerus*) and could represent a new synapomorphy for a subclade of Cryptoclididae (see Discussion). The dorsal surface of the frontal in PMO 224.248 is generally smooth, but is textured with a few small indentations adjacent to the interfrontal vacuity.

The morphology of the ventral surface of the frontal in *Ophthalmothule cryostea* is visible in the µCT images and tapers medially in cross section. On the ventral surface of the frontal in *Kimmerosaurus langhami*, *Cryptoclidus eurymerus* and *Muraenosaurus leedsii* a trough is present on either side of the interfrontal vacuity or frontal midline. In *K. langhami* these are clearly seen, starting posteriorly in line with the pineal foramen and terminate at the preserved anterior end of the frontal (*pers. obs.* AJR NHMUK R8431). These structures are absent in *Tricleidus seeleyi* and *O. cryostea* based on the µCT images.

The frontal-parietal suture is somewhat obscured in dorsal view due to gypsum mineralization and the presence of rugosities in the anterior portion of the parietal. However, µCT images show that the posterior margin of the frontal interdigitates with the anterior margin of the parietal and that the frontal envelopes the anterior rim and most of the lateral rims of the pineal foramen (Fig. 6).

Parietal

The anterior extent of the parietal lies approximately in line to the level of the temporal bar. In dorsal view, the parietal bears a mediolaterally narrow sagittal crest that is slightly flattened dorsally, exhibiting an intermediate condition between the tall and sharp crest seen in *Cryptoclidus eurymerus* (Brown and Cruickshank, 1994) and the broad, flat sagittal crest seen in *Kimmerosaurus langhami* (Brown, 1981). In lateral view, the apex of the sagittal crest is straight

and gently inclines posterodorsally. In contrast, this morphology differs from the dorsally convex sagittal crest seen in *C. eurymerus*. The squamosal-parietal contact is indiscernible.

The μCT images reveal the presence of two large dorsoventrally oriented fossae in the parietals that open onto the posteroventral surface, but do not extend to the dorsal surface (Fig. 6). This feature is also present in another undescribed Slottsmøya Member cryptoclidid (PMO 212.662). In *Kimmerosaurus langhami* (NHMUK R.8431), these parietal fossae are likely absent, as they are not visible on the ventral surface (Brown, 1981). In *Cryptoclidus eurymerus* (NHMUK R.2860) and *Muraenosaurus leedsii* (NHMUK R.2422) the parietals are partly obscured by the supraoccipital and parietal fossae cannot be identified. Although the function of these fossae is currently unclear, CT scanning of additional specimens could infer whether this is a cryptoclidid feature or more constrained to a specific clade.

Squamosal

In lateral view, the suspensorium is near vertically inclined, although the dorsal half of the squamosal dorsal ramus is inflected abruptly anteriorly (supplementary information, Fig. S.2). The squamosal bears a dorsoventrally tall anterior ramus which curves slightly medially, following part of the anterior margin of the temporal fenestra. The ventromedial process of the squamosal is short, extending ventrally to roughly half the dorsoventral length of the quadrate shaft. The dorsal margin of the squamosal-quadrate suture is visible in posterior view, where a small groove is present (Fig. 7). However, this suture could not be located dorsally in μCT scan images (supplementary information 6, Fig. S.2). The relationships between the squamosal and the jugal and postorbital cannot be discerned due to poor preservation in this area.

Quadrate

Due to a fracture running along the middle of the right quadrate, the left quadrate is better preserved. Similar to *Djupedalia engeri* and *Kimmerosaurus langhami*, the lateral cotyle of the quadrate condyle in *Ophthalmothule cryostea* is slightly larger in anteroposterior length and dorsoventral extent than the medial cotyle (Brown, Milner and Taylor, 1986; Knutsen, Druckenmiller and Hurum, 2012a). This differs from *Spitrasaurus larseni*, where the opposite state is present (Knutsen, Druckenmiller and Hurum, 2012b). There is no indication of a quadrate foramen.

Basioccipital

The anterior and dorsal surfaces of the basioccipital of *Ophthalmothule cryostea* are obscured by matrix and other skull elements, but can be described fully using the µCT segmentation (Fig. 8). The occipital condyle lacks both a notochordal pit and a constriction on the dorsal and ventral surfaces; however, a slight constriction is visible on the lateral surfaces. As in *Spitrasaurus larseni*, the exoccipital facets reach, but do not contribute to the occipital condyle (Knutsen, Druckenmiller and Hurum, 2012b). In contrast, the exoccipitals in *Kimmerosaurus langhami* and in some specimens of *Cryptoclidus eurymerus* form a portion of the condyle (Andrews, 1910; Brown, 1981). In posterior view, the condyle is mediolaterally wider than dorsoventrally tall. The height-to-width ratio (H/W) of the condyle (~0.82) is comparable to that of *Spitrasaurus larseni* (0.8) and *Kimmerosaurus langhami* (0.85) (Knutsen, Druckenmiller and Hurum, 2012b), but differ from *Muraenosaurus leedsii* and *T. seeleyi* that possess more circular condyles (H/W ~1).

Similar to *Tricleidus seeleyi* and another undescribed Slottsmøya Member cryptoclidid specimen (PMO 212.662), the basioccipital tubera of *Ophthalmothule cryostea* are dorsoventrally flattened and triangular in general outline as seen in ventral view and their ventral surfaces are gently concave in occipital view (supplementary information, Fig. S.2). The entire anterolateral margin of the tubera meet and run parallel to the pterygoid extending to the basisphenoid margin. This morphology contrasts to the pillar-like (circular in cross section) and laterally-facing tubera in *Cryptoclidus eurymerus* and *Kimmerosaurus langhami (*Andrews, 1910; Brown, 1981). In addition to this morphology, *K. langhami* displays finished bone along the posterolateral basioccipital margin between the basisphenoid facet and tubera (Brown, 1981; Brown and Cruickshank, 1994).

The posterior floor of the foramen magnum is visible, forming part of a shallow but mediolaterally broad concavity between the two exoccipital-opisthotics. Anteriorly, there is a low anteroposteriorly oriented ridge that terminates near the contact with the basisphenoid (Fig. 8B). Two paired foramina open on to the dorsal surface of the basioccipital and extend into the body of the element, where they are visible in the µCT images, but terminate before reaching the ventral surface. Similar to *Kimmerosaurus langhami*, the ventral surface of the basioccipital is relatively flat, with a short anteroposteriorly oriented median ridge that terminates at the rim of the anterior margin (Brown, 1981).

409 ***Parabasisphenoid***

410 The demarcation between the parasphenoid and basisphenoid of PMO 224.248 is indiscernible. In
411 dorsal view on the posterior margin of the body of the parabasisphenoid, a small fossa is present
412 along the suture with the basioccipital ('dmp', Fig. 8A). This structure appears homologous with
413 the "dorsal median pit" described in *Muraenosaurus leedsii* (Andrews, 1910), hypothesised to
414 mark the embryonic basicranial fenestra. However, the foramen present in PMO 224.248, is
415 significantly reduced in comparison to *M. leedsii* (Andrews, 1910). A deep fossa is present on the
416 anterior margin of the basisphenoid body interpreted to be the pituitary (or hypophyseal) fossa,
417 similar to that described in *Tricleidus seeleyi*, *Kimmerosaurus langhami* and *M. leedsii* (Andrews,
418 1910; Brown, Milner and Taylor, 1986). The ventral floor of the pituitary fossa, including parts of
419 both the basisphenoid and parasphenoid (Andrews, 1910), is missing likely due to taphonomic
420 loss. In lateral view the internal carotid foramen is visible opening into the pituitary fossa (not
421 visible on right). In dorsal view on the posterior margin of the parabasisphenoid, a small fossa is
422 present along the suture with the basioccipital. In palatal view, the basal articulation of
423 plesiosauroids is often visible in ventral view through the posterior interpterygoid vacuity (Buchy,
424 Frey and Salisbury, 2006). In PMO 224.248, the basal articulation is visible on the µCT scans and
425 is better preserved on the left side and positioned dorsally in respect to the rest of the palate.

426 The parabasisphenoid bears posterolaterally located facets for the anteromedial process of
427 the pterygoid similar to *Tricleidus seeleyi*, but in contrast to *Muraenosaurus leedsii* and
428 *Cryptoclidus eurymerus* where the pterygoid simply articulates to the basioccipital tuber
429 (Andrews, 1910; Brown, 1981). In *T. seeleyi*, the pterygoid facets of the parabasisphenoid are
430 circular in outline and are slightly anterolaterally projecting, whereas in PMO 224.248 the facet
431 surface appears uniform and triangular in shape in the µCT images. The presence of a pterygoid
432 facet on the body of a parabasisphenoid is also present in another Slottsmøya Member cryptoclidid
433 (PMO 212.662) and has been suggested to be present in *Kimmerosaurus langhami* (NHMUK
434 R10042; Benson and Druckenmiller, 2014: Appendix S2). That a minimum of three cryptoclidid
435 taxa share this palatal configuration over a long temporal span (Callovian – Volgian), suggests that
436 this morphology is more widespread in cryptoclidids than previously believed.

437 Anteriorly, the parabasisphenoid is very thin and somewhat damaged, making this region
438 difficult to segment out of the µCT images. The anterior portion (parasphenoid) separates the

pterygoids along the midline and forms the entire posterior margin of the anterior interpterygoid vacuity, but lacks a projecting cultiform process, like that seen in some polycotylids and basal plesiosaurians (Buchy, Frey and Salisbury, 2006; Carpenter, 1996; O'Keefe, 2001; Vincent and Benson, 2012). The anterior margin of the posterior interpterygoid vacuity is formed by a lateral extension of the parabasisphenoid.

Exoccipital-opisthotic

Both exoccipital-opisthotics are preserved in partial articulation, but are damaged and displaced venterolaterally due to compression. As only the posterior view of these elements is visible on the specimen (Fig. 7), the following description is largely based on μCT images (Fig. 9).

The body of the exoccipital-opisthotic in *Ophthalmothule cryostea* is dorsoventrally taller than mediolaterally wide. In posterior view, the paraoccipital process is visible extending laterally from the body of the element. The cross-sectional shape of the paraoccipital process shaft is dorsoventrally taller than wide. Similar to *Muraenosaurus leedsii*, the length of the paraoccipital process is close to the dorsoventral height of the exoccipital, in contrast to *Tricleidus seeleyi* and *Djupedalia engeri*, which have more elongate paraoccipital processes (Andrews, 1910; Brown, 1981; Knutsen, Druckenmiller and Hurum, 2012a). As in *Kimmerosaurus langhami* and *Cryptoclidus eurymerus*, the paraoccipital process is expanded distally where it contacts the squamosal (Brown, 1981).

On the medial surface, a large anteroposteriorly oriented cavity is present at the centre of the exoccipital-opisthotic body. Although the structure is distorted, it may represent the recess for the utriculus as described for *Muraenosaurus leedsii* and *Tricleidus seeleyi* (Andrews, 1910). Two semicircular canal openings are visible in medial view: a dorsally orientated vertical posterior semicircular canal and a horizontal anterior semicircular canal. The posterior vertical semicircular canal is positioned just anterior to the supraoccipitial facet and runs ventrally into a cavity interpreted to be for the utriculus, similar to *Kimmerosaurus langhami* and *Cryptoclidus eurymerus* (Andrews, 1910; Brown, 1981). The horizontal anterior semicircular canal is located directly ventral to most of the prootic facet and opens posteriorly into the utricular cavity.

In lateral view (Fig. 9B), a large foramen could either be for the exit for cranial nerve X, or may be formed of multiple cranial nerve openings which have merged due to crushing. The

posterior portion of the fenestra ovalis is located along the anterior margin of the exoccipital, ventral to anterior horizontal canal and the prootic facet.

Supraoccipital

The supraoccipital remains in articulation with the parietal, but has rotated anteriorly so that its posterior surface faces dorsally. The element is anteroposteriorly thickest at the exoccipital-opisthotic facet and thins dorsally. Compared to the relative dorsoventral height of the exoccipital-opisthotic, the supraoccipital contributes roughly half of the total height of the foramen magnum. The foramen magnum appears to be oval in shape, unlike the more hour-glass outline seen in *Kimmerosaurus langhami* (Brown, Milner and Taylor, 1986). *Ophthalmothule cryostea* lacks a posteromedian ridge on the supraoccipital, as seen in *K. langhami* and *Muraenosaurus leedsii* (Brown, Milner and Taylor, 1986). A small foramen located on the midline of the dorsal border with the parietal, a feature that is also present in *C. eurymerus* (Brown, 1981, Fig. 2), but notably absent in *M. leedsii* and possibly *K. langhami* (Brown, 1981; Brown, Milner and Taylor, 1986; AJR *pers. obs.* NHMUK R.10042).

Prootic

Two crushed and slightly disarticulated elements visible anterior to the exoccipital-opisthotics in the µCT images, are interpreted to be the prootics (Fig. 8). The elements are too distorted to warrant further description.

Vomer

The anterior extent of the vomers in *Ophthalmothule cryostea* (PMO 224.248) is unclear, however they are mediolaterally narrowest anteriorly. Posterior to the internal nares, the vomer expands in mediolateral width, becoming broadest near their posterior margin, similar to that observed in *Muraenosaurus leedsii* (Andrews, 1910). The left and right vomers are in full contact along the midline, though unfused and the ventral surface is convex and lacks ornamentation. This differs from the clear fusion seen in *Vinialesaurus caroli* (Gasparini, Bardet and Iturralde-Vincent, 2002) and partial fusion and ridged ventral surface in an undescribed juvenile Callovian cryptoclidid specimen (NHMUK R 2853; *pers obs.* AJR). As in most other cryptoclidids, the vomer forms the medial and at least part of the anterior border (Andrews, 1910). As in some other plesiosauroids that preserve this region (e.g. *M. leedsii*; Andrews, 1910), the vomers have posterolaterally

497 expanded margins that partially lie ventral to the palatines, an orientation confirmed by the µCT
498 images in cross section. The posterior contact with the pterygoids consists of an interdigitating
499 suture. The vomer forms the anterior border of the anterior interpterygoid vacuity, in contrast to
500 *M. leedsii* and *Cryptoclidus eurymerus* where the pterygoids meet anteriorly along the midline and
501 exclude the vomer from participation in margin of the anterior interpterygoid vacuity (Andrews,
502 1910; Brown and Cruickshank, 1994).

503 ***Palatine***

504 The palatine of *Ophthalmothule cryostea* form the posterolateral border of the internal naris. As is
505 typical of cryptoclidids, the palatines do not meet anteriorly along the midline, but are separated
506 anteriorly by the vomer (Buchy, Frey and Salisbury, 2006). Similar to *Cryptoclidus eurymerus* and
507 *Muraenosaurus leedsii* a suborbital fenestra is absent (Andrews, 1910; Brown and Cruickshank,
508 1994). The posterior margin of the palatine is presumed to terminate at the anterior margin of the
509 ectopterygoid, although it is difficult to discern the nature of this contact due to poor preservation
510 in this area. The ectopterygoid area lacks a boss or flange of the pterygoid.

511 ***Pterygoid***

512 The pterygoid of *Ophthalmothule cryostea* is mediolaterally narrow anteriorly and gradually
513 increases in width posteriorly, as in *Cryptoclidus eurymerus* and *Muraenosaurus leedsii* (Andrews,
514 1910; Brown, 1981; Brown and Cruickshank, 1994). The anterior region of the pterygoids is
515 separated along the midline, by a prominent and mediolaterally broad anterior interpterygoid
516 vacuity. The mediolaterally broad morphology of the anterior pterygoid vacuity is similar to
517 *Tricleidus seeleyi* and does not narrow anteriorly to the same degree as in *Muraenosaurus leedsii*
518 (Andrews, 1910).

519 The pterygoid forms the lateral margins of the posterior interpterygoid vacuity, which is
520 anteroposteriorly short compared to *Cryptoclidus eurymerus* and *Muraenosaurus leedsii*
521 (Andrews, 1910; Brown, 1981). The pterygoids do not meet along the midline posterior to the
522 posterior interpterygoid vacuity, as is the case in some leptocleidids and polycotylids (e.g.
523 *Edgarosaurus muddi*, *Umoonasaurus demoscyllus*; Druckenmiller, 2002; Kear, 2006). The
524 posterior interpterygoid vacuity is located entirely posterior to the anterior margin of the
525 subtemporal fossa, as in *Tricleidus seeleyi* (Andrews, 1910).

As in *Tricleidus seeleyi*, the pterygoid bears a narrow, prong-like anteromedial process (basisphenoid process of the pterygoid; Andrews 1910) that contacts the parabasisphenoid. The anteromedial process parallels the anterolateral margin of the basioccipital, but does not form a distinct facet for it. The anteromedial process in *Ophthalmothule cryostea* is similar in relative length to that of *T. seeleyi*; however, it differs from *T. seeleyi* in being anteromedially curved rather than straight and greater in dorsoventral height (based on CT imaging) in lateral view (Andrews, 1910).

The quadrate ramus of the pterygoid deflects posterolaterally towards the pterygoid ramus of the quadrate and is dorsoventrally taller than wide. The pterygoid forms a broad medially facing facet for the quadrate, similar to *Kimmerosaurus langhami* (Brown, 1981).

Mandible

Each mandibular ramus is disarticulated from the cranium of PMO 224.248 and the anterior portions of each are missing, including the symphyseal region (Fig. 10). Based on corresponding measurements from the upper jaws, the left mandible lacks the anterior 10.5 cm of the ramus, providing an estimated total mandibular length of 27 cm.

The left mandible, which is more complete and the basis for the following description, preserves the dentary, splenial, angular, surangular and articular (see supplementary information Fig. S.3). The Meckalian canal is visible on the left mandible, suggesting that the prearticular and splenial are damaged. A disarticulated element either representing the prearticular or splenial is present adjacent to the right mandible (supplementary information, Fig. S.4). There is no visible facet or suture on the surangular for the coronoid, as seen clearly in *Tricleidus seeleyi* (Andrews, 1910; Brown, 1981).

In dorsal view, the alveolar row is laterally positioned relative to the parasagittal long axis of the ramus, resulting in a mediolaterally expanded dorsal portion of the dentary that preserves fourteen alveoli (inferred from µCT images). The alveoli are strongly labially angled (~60° from the parasagittal plane), which increases slightly anteriorly. This differs from the more dorsally-directed alveoli in *Tricleidus seeleyi* (Andrews, 1910). In dorsal view, only a couple of the primary alveoli for the replacement teeth are visible, as these are partially covered by matrix. The mediolateral expansion of the dentary preserves finished bone medial to the alveoli, contributing

to at least a third of the lateromedial width of the dentary dorsal surface. Ventrally, the mediolateral expansion abruptly decreases in width. In cross section, the anterior portion of the element (at the mid-point of the dentary) is subtriangular due to the expanded mandibular dorsal surface. Similar expanded mediolateral dorsal surfaces are also observed in *Spitrasaurus larseni*, *Djupedalia engeri* and *Muraenosaurus leedsii* (Andrews, 1910; Knutsen, Druckenmiller and Hurum, 2012a; Knutsen, Druckenmiller and Hurum, 2012b). In *Kimmerosaurus langhami* a mediolaterally expansion of the dentary is present although possibly due to taphonomy in one of the referred specimens (NHMUK R.10042; *pers. obs.* AJR), but it appears absent on the holotype specimen (Brown 1981). This morphology differs from the other taxa, where a mediolateral expansion is either missing entirely (*Tricleidus seeleyi*), or a lateral expansion is only present on the posterior half of the dentary (*Cryptoclidus eurymerus*; '*Picrocleidus*' *beloclis*) and lacks the abrupt ventral constriction observed in *Ophthalmothule cryostea*, *S. larseni* and *Muraenosaurus leedsii* (Andrews, 1910; Brown, 1981; Knutsen, Druckenmiller and Hurum, 2012b). This feature is proposed as a new phylogenetic character (see Discussion).

The lateral surface of the dentary is gently striated. Dorsomedially, a partial suture between the splenial and dentary is visible. Posteriorly, there is no clear suture between the dentary and surangular. The angular-surangular suture is partly visible in lateral and medial views. In *Kimmerosaurus langhami* and *Cryptoclidus eurymerus* the ventral margin of the angular is convex ventral to the glenoid, becoming concave anteriorly along the ventral margin (Brown, 1981; Brown and Cruickshank, 1994). This morphology is reduced in PMO 224.248 and *Tricleidus seeleyi*, where the ventral margin of the angular is almost straight, with a slight convexity in line with the articular (Andrews, 1910; Brown, 1981). The surface of the glenoid is slightly undulated posteriorly and dorsoventrally deep, being over half the dorsal-ventral height of the mandible. This is distinct from the shallow and smooth articular facet of *Colymbosaurus*, *Cryptoclidus eurymerus*, *Muraenosaurus leedsii* and *Kimmerosaurus langhami* (Brown, 1981; Roberts et al., 2017).

In *Ophthalmothule cryostea*, the retroarticular process is uniform in dorsal-ventral thickness until it reaches the posterior terminus. The retroarticular process is nearly twice as long as it is dorsoventrally tall, in contrast to the ~~even~~ longer than tall retroarticular process in *Spitrasaurus larseni* (Knutsen, Druckenmiller and Hurum, 2012b) and *Muraenosaurus leedsii* (Andrews, 1910). The process is dorsally inclined at ~15º with respect to the longitudinal axis of

585 the mandibular ramus. This is significantly less than the in strong inclination seen in *S. larseni*
586 (35º) and greater than *Colymbosaurus indet.* (OUM J. 3300; ~9°) and *Tricleidus seeleyi* (10º;
587 Brown, 1981). A mediolateral deflection of the retroarticular process is absent.

588 ***Dentition***

589 Eight partial to complete but displaced teeth, along with several fragments were found adjacent to
590 the anterior region of the skeleton. Fully erupted teeth are absent in all of the dentigerous portions
591 preserved in PMO 224.248, but several unerupted replacement teeth are visible *in situ* on the µCT
592 images. The individual teeth vary slightly in size, but not morphology, indicating that the minor
593 size difference represents stages of tooth replacement and not heterodonty as suggested by the
594 alveoli. The crowns are gracile in comparison to the more robust teeth in *Tricleidus seeleyi* and
595 *Cryptoclidus eurymerus* (Brown 1981). The largest and most complete tooth preserved (Fig. 11A),
596 measures ~4 cm in length from apex of the crown to the root. In axial (mesial/distal) view, the
597 complete tooth (Fig. 11A), is lingually curved along the crown, straightens at the start of the root
598 and terminates in a slightly lingually curved root terminus. This morphology differs from the
599 significantly lingually curved teeth of *Kimmerosaurus langhami* (75º; Brown, 1981) and
600 *Spitrasaurus larseni* Knutsen, Druckenmiller and Hurum, 2012b). The enamelled crown
601 represents a third of the total length of the tooth and displays a gradual transition to the root. A
602 smaller, but fractured tooth (Fig. 11B-E), bears fine longitudinal ridges on the enamel, which
603 gradually fades towards the apex. The ridging is most prominent on the labial side, unlike the
604 prominently lingually ridged teeth of *Muraenosaurus leedsii* and *Cryptoclidus eurymerus* (Brown,
605 1981). On some teeth, the axial (mesial?/distal?) margin of the crown bears a more pronounced
606 enamelled ridge. This ridge could represent the edge of a partial wear facet, as it has no distinct
607 shared morphology between teeth and has a variable presence on the preserved tooth crowns
608 (supplementary information, Fig. S.5). Close to the tip of the crown, the labial side is flattened
609 compared to the convex lingual surface resulting in a D-shaped cross section, similar to
610 *Spitrasaurus larseni* and some elasmosaurids (Knutsen, Druckenmiller and Hurum, 2012b; Sato,
611 Hasegawa and Manabe, 2006). This morphology differs from the more oval-shaped cross section
612 in *K. langhami*, *M. leedsii* and *C. eurymerus* (Brown 1981). The shaft of the root is subcircular in
613 cross section and slightly expanded in diameter at the start of the crown, by a gently undulating
614 surface that decreases in width towards the root ~~terminus.~~ One of the teeth (supplementary

information, Fig. S.5), has a clear reabsorption facet on the lingual side of the root. The root terminus is straight and abrupt, whereas other cryptoclidids show a more gradual reduction in diameter at the root terminus (e.g. *K. langhami* and *C. eurymerus*; PETMG R.283.412).

Axial skeleton

Fifty cervical vertebrae are preserved in PMO 224.248, including the atlas-axis complex. This is greater than in Callovian cryptoclidids (*Cryptoclidus eurymerus*, 32: Brown, 1981; *Muraenosaurus leedsii,* 44: Brown, 1981) and some Tithonian – Early Cretaceous taxa (*Colymbosaurus megadeirus,* 41: Benson and Bowdler, 2014; *Abyssosaurus,* 44-51: Berezin, 2011; *Djupedalia engeri,* >40: Knutsen, Druckenmiller and Hurum, 2012a). PMO 224.248 preserves fewer cervical vertebrae than that described in *Spitrasaurus wensaasi* (60; Knutsen, Druckenmiller and Hurum, 2012b). In total, the neck of PMO 224.248 is estimated to be approximately 2 m in length including the preserved intervertebral spacing prior to preparation. Selected measurements from the axial skeleton can be found in the supplementary information, (Table S2).

Atlas-axis

Reflecting the advanced ontogenetic status of PMO 224.248, the atlas-axis complex is completely fused; however, part of the suture between the atlas and axis centrum remains visible (Fig. 12). The complex is approximately twice as anteroposteriorly long as mediolaterally wide, whereas in *Spitrasaurus larseni* and *Colymbosaurus megadeirus*, the complex is only slightly anteroposteriorly longer than wide (Benson and Bowdler, 2014; Knutsen, Druckenmiller and Hurum, 2012b). The long and narrow morphology of the atlas-axis in *Ophthalmothule cryostea* is more similar to that of *Muraenosaurus leedsii* and some elasmosaurids, such as *Aristonectes parvidens* (Andrews, 1910; Brown, 1981; Gasparini et al., 2003).

In anterior view, the atlantal cup is concave and subcircular in outline. In the absence of a visible suture, it is not possible to confirm atlantal centrum (odontoid) participation in the ventral portion of the atlantal cup, a feature common in cryptoclidids, including C*olymbosaurus megadeirus* and *Spitrasaurus* (Benson and Bowdler, 2014; Knutsen, Druckenmiller and Hurum, 2012b). Ventrally, the atlantal intercentrum forms a low anteroventrally directed hypophyseal eminence, similar to *C. megadeirus*, *Spitrasaurus* and *Abyssosaurus nataliae* (Benson and

Bowdler, 2014; Berezin, 2011; Knutsen, Druckenmiller and Hurum, 2012b), that is positioned in the anterior half of the element, although this is positioned more centrally in *C. megadeirus* (Benson and Bowdler, 2014). This morphology differs from the ventral keel formed by the ventral surface of the atlas present in the Oxford Clay Formation cryptoclidids and elasmosaurids (Andrews, 1910; Gasparini et al., 2003).

As in most cryptoclidids (with the exception of *Colymbosaurus megadeirus*) an atlantal rib is present and is set posteriorly on the atlas centrum (Benson and Bowdler, 2014). The axial rib is single-headed and occupies most of the ventrolateral length of the axial centrum, where it is fused. This differs from *C. megadeirus*, where the axial rib is borne partly on the posterolateral portion of the atlantal centrum (Benson and Bowdler, 2014). The ventral surface of the axis is generally concave, with a rounded, low and anteroposteriorly orientated ridge running from the anterior edge of the axis. The neural arch of the atlas-axis complex is fused and bears a dorsoventrally short, but anteroposteriorly elongate neural spine.

Cervical vertebrae (3-50)

The articular surfaces of the centra are weakly amphicoelous, although not to the degree of concavity observed in *Kimmerosaurus langhami* (Brown, Milner and Taylor, 1986). The anterior cervical vertebrae are mediolaterally wider than anteroposteriorly long (supplementary information, Table S2). This relationship shifts gradually in the mid-cervical region as the length to width ratio steadily decreases posteriorly. The posterior cervical vertebrae (~35 – 50) are mediolaterally wider than anteroposteriorly long, unlike the more equal dimensions seen in *Cryptoclidus eurymerus* (Andrews, 1910) and a partial cryptoclidid specimen from Greenland (MGUH 28378; Smith, 2007).

The lateral surfaces of the anterior centra are conspicuously concave, becoming more convex posteriorly in the series (Fig. 13). A structure that could represent a ~~weak~~ lateral ridge is present in some of the mid-posterior cervical vertebrae in *Ophthalmothule cryostea* and is visible in the cervical vertebrae 32-38 (Fig. 14). This should not be confused with the raised convex dorsal margin of the rib facet, which is present in most of the cervical vertebrae. This transverse ridge crosses the lateral surface of the centrum, positioned in between the neural arch pedicles and rib facet. A lateral ridge may have been present in more anterior/posterior vertebrae, but cannot be unambiguously identified due to the preservation. In *Spitrasaurus*, a lateral ridge is present

throughout most of the cervical series, located dorsal to the cervical rib facet (Knutsen, Druckenmiller and Hurum, 2012b). The ventral surface of the anterior – middle cervical vertebrae bear paired foramina separated by a sharp ridge in the anterior cervicals, which disappears posteriorly in the series. The presence of a ventral ridge is shared with some cryptoclidids (e.g., *Tricleidus seeleyi*; Andrews, 1910), but is completely absent in *Colymbosaurus megadeirus* (Benson and Bowdler, 2014).

In dorsal view, the prezygapophyses are mediolaterally narrower than the width of the centrum and positioned directly above the centrum, similar to *C. megadeirus*, *Abyssosaurus nataliae* and *Djupedalia engeri* (Benson and Bowdler, 2014; Berezin, 2011; Knutsen, Druckenmiller and Hurum, 2012a). Similar to *Kimmerosaurus langhami* (Brown, Milner and Taylor, 1986), in the anterior-most cervicals (3-6) of PMO 224.248, the prezygapophyses are separate along their entire length. However, in the following cervicals the prezygapophyses partially fuse medially along the anteroventral margin beginning approximately at cervical 15, the prezygapophyses are completely fused medially. This morphology differs from *Spitrasaurus* spp. and *Djupedalia engeri*, where the prezygapophyses are either partially or completely ventrally fused throughout the entire neck (Knutsen, Druckenmiller and Hurum, 2012a; Knutsen, Druckenmiller and Hurum, 2012b). In *Cryptoclidus eurymerus* the prezygapophyses remain unfused (Andrews, 1910; Brown, 1981). As in *Spitrasaurus*, the postzygapophyses are fused throughout the entire cervical series and extend posterior to the posterior margin of the centrum. In PMO 224.248, the length of the postzygapophyses varies throughout the series and in some regions significant posterior elongation is preserved: on the eighth cervical, the postzygapophysis length approaches the anterior-posterior length of the entire centrum (supplementary information, Fig. S.6). When articulated with the ninth cervical, there is a larger intervertebral space in between the two centra, than in preceding and following cervical vertebrae. Based on studies of sauropod dinosaurs, this could represent an area of more flexibility in the neck (Taylor and Wedel, 2013).

The neural spines in the anterior-most cervical vertebrae (3-10) are low, anteroposteriorly extended and angled posteriorly, being positioned over the postzygapophyses. Where the neural spine is completely preserved, the dorsal margin is slightly rounded. This morphology differs from the relatively straight, tall and dorsally flattened margins of the neural spines of the anterior-most cervical vertebrae in *Kimmerosaurus langhami, Spitrasaurus* and *Djupedalia engeri* (Brown,

Milner and Taylor, 1986; Knutsen, Druckenmiller and Hurum, 2012a; Knutsen, Druckenmiller and Hurum, 2012b). In the 7th cervical, the neural spine is less than half the dorsoventral height of the centrum, when measured from the top of the postzygapophyses. The anterior – mid cervical neural spines (10-18) are posteriorly shifted~~,~~ so that the middle of the dorsal margin of neural spine is positioned directly over the posterior margin of the centrum (Fig. 13F). In lateral view the neural spines are triangular to trapezoid in outline, becoming more rectangular posteriorly and increase in height. The neural spines on the posterior cervicals are anteroposteriorly long, dorsally flattened and more centred over the centrum. Although positioned more centrally, the posterior margin of the neural spine still reaches the anterior half of the next centrum due to the anteroposterior length of the neural spine (Fig. 14). Some of the mid and the posterior cervicals show a mild anterior inclination of the neural spine. This morphology is comparable to that seen in *Spitrasaurus wensaasi* and "*Picrocleidus*" *beloclis*; however, the neural spines of *Ophthalmothule cryostea* do not consistently angle anteriorly as in *Spitrasaurus* spp. (Knutsen, Druckenmiller and Hurum, 2012b). The neural canal is oval in anterior view.

Cervical ribs

The cervical rib facets receive single-headed ribs, which are fused to the centrum throughout the entire series (Figs. 13-14). In the anterior cervicals, the cervical ribs are relatively short, hatchet-shaped due to a small anterior process and terminate laterally in a posterodistal point. In the mid-cervical vertebrae, the anterior process is further reduced, gradually increasing in prominence in the posterior cervicals. This differs from *Djupedalia engeri*, where the anterior process on the cervical ribs is clearly present in the entire cervical series (Knutsen, Druckenmiller and Hurum, 2012a). In the mid-cervicals, the ribs are distally short and lack anteroposterior curvature. From the 40th cervical, the ribs start to elongate exceeding the length of the centrum. Similar to *Djupedalia engeri*, the posterior cervical ribs become anteroposteriorly narrower and curve posteriorly (Knutsen, Druckenmiller and Hurum, 2012a). This morphology differs from MGUH 28378 (*Cryptoclididae* indet.), where the posterior cervical ribs are straight and to *Spitrasaurus wensaasi*, where they are only slightly posteriorly curved (Knutsen, Druckenmiller and Hurum, 2012b; Smith, 2007). From the 44th cervical and posteriorly, the cervical ribs bear a longitudinal, dorsally positioned ridge, starting from the proximal head and terminating around the midpoint of the rib shaft, an autapomorphy of this taxon. This longitudinal ridge is also present on the pectoral

and anterior dorsal ribs and represents a muscle attachment site (Noè, Taylor and Gómez-Pérez, 2017).

Pectoral vertebrae

At least two pectoral vertebrae (Fig. 15A-F) can be unambiguously identified (*sensu* Sachs, Kear and Everhart, 2013), with the possibility of a third (Fig. 15G). As in *Colymbosaurus megadeirus* (Benson and Bowdler, 2014), the centra are significantly mediolaterally wider than dorsoventrally tall in anterior view (supplementary information, Table S2), although this may be partially due to taphonomic compression. As in *Cryptoclidus eurymerus*, pectoral vertebrae 1 and 2 have clear circular rib facets and the subcentral foramina are widely spaced compared to the cervicals (Brown, 1981). The neural arch is poorly preserved and cannot be described in detail. A third poorly preserved vertebra could represent the third pectoral (Fig. 15G). This element was slightly disarticulated posteriorly from the two pectorals and located just posterior to the medial symphysis of the scapula during preparation. The neural arch and centrum contribute to the dorsoventrally tall and laterally extended rib facet, which almost forms a transverse process on the right side. This rib facet morphology is also present in the pectoral and sacral vertebrae of *Colymbosaurus megadeirus* (CAMSM J.29640; Benson and Bowdler, 2014). As such the location and similar morphology to other posterior pectorals in *Colymbosaurus*, supports the argument that this element can be identified as the third pectoral vertebrae.

Several pectoral ribs are preserved, either in articulation with or adjacent to the pectoral vertebrae. These share the same morphology as the posterior cervical ribs, but are more distally elongate.

Dorsal vertebrae

Ten dorsal vertebrae are preserved, however, the posterior-most of these are poorly preserved and some are fused together by diagenesis (Fig. 16). The dorsal vertebrae are mediolaterally narrower than the posterior-cervical and pectoral vertebrae but not to the degree as in *Spitrasaurus wensaasi* (Knutsen, Druckenmiller and Hurum, 2012b). The neural arches are crushed and the transverse processes flattened; however, taking into account the shape of the dorsal rib heads and deformation of the transverse process, the rib facets are dorsoventrally taller than wide, being oval in outline as in *Spitrasaurus wensaasi* (Knutsen, Druckenmiller and Hurum, 2012b). This contrasts to the more

circular dorsal rib facets described in *Tatenectes* and most Oxford Clay Formation cryptoclidids (Andrews, 1910; O'Keefe et al., 2011). The anterior dorsal centra preserve either singular or paired subcentral foramina on the ventrolateral surface.

Dorsal ribs

The majority of the dorsal ribs are incomplete due to erosion. Two ribs remain complete(an anterior- (Fig. 16I) and a mid-dorsal rib), but are somewhat crushed. The rib heads are robust and single headed with an oblong ovoid facet (Fig. 16H), being dorsoventrally taller than anteroposteriorly wide as in *Colymbosaurus megadeirus* (Benson and Bowdler, 2014) and a specimen referable to *Muraenosaurus* (NHMUK R.2427). The mid-dorsal rib was in partial-articulation with the 5th dorsal vertebrae and is 66.5 cm in actual length. This rib is curved along the proximal half of the shaft and then straightens out towards the expanded distal end. On the proximal end, a ridge is present on the posterolateral margin. The cross section is subcircular in shape along most of the shaft, but increases in mediolateral width proximally. A groove is present on the posterior surface of the proximal and distal regions of the rib. On the anterior dorsal ribs a longitudinal ridge is present, as described for the posterior cervical- and pectoral ribs.

Gastralia

The gastral basket of PMO 214.248 is well-preserved, with at least ten sets of gastralia identified. These form a tight gastral basket, where the first set butts against the posterior margin of the coracoid. Each set contains a medial gastralium, which in turn articulates with 2-3 lateral gastralia on either side. Some of the gastralia are partially fused, which is attributed to the sideritic cement covering the dorsal surface.

Gastroliths and stomach content

The posterior region of the gastral basket, was covered in a rusted silt layer in PMO 214.248. This sediment predominately silty matrix includes a large number of small worn pebbles and bone fragments; thus, we interpret this area as stomach contents containing possible gastroliths. The "gastroliths" are small, ranging from <2cm in diameter and are significantly smaller than those described from Late Cretaceous elasmosaurids (Cicimurri and Everhart, 2001; Everhart, 2000). A section of the layer along with a section of the underlying gastralia was µCT scanned, revealing a large amount of material embedded in the matrix. To our knowledge, this is the first time

gastroliths have been described for cryptoclidid plesiosaurs. However, due to the small size of the pebbles, it may suggest these are simply picked up during feeding in bottom sediments (Noè, Taylor and Gómez-Pérez 2017). The material requires further analysis to derive the source of the gastroliths and the origin of the bone material, which is beyond the scope of this paper.

Appendicular skeleton

Clavicle and interclavicle

Two clavicles and an interclavicle are preserved in articulation with the scapula. Due to the hard matrix in this region, it was not possibly to separate the elements from the scapula and overlying vertebrae. The clavicles (dorsal to interclavicles) are only visible in cross section, are dorsoventrally thin and are reduced in comparison to the interclavicle, as in *Muraenosaurus leedsii* (Andrews, 1910; Brown, 1981). The interclavicle forms the anterior-most margin of the pectoral girdle along the midline, resembling the triangular element present in *Muraenosaurus leedsii* (Andrews, 1910; Brown, 1981).

Scapula

The scapulae of PMO 224.248 are preserved in articulation with the rest of the pectoral elements and humeri (Fig. 17). Selected measurements of these elements can be found in supplementary information, Table S3. The anterior and medial margins of the scapulae are difficult to interpret, due to poor preservation and crushing by overlying elements (clavicles, interclavicle). As in all adult cryptoclidids with the exception of *Abyssosaurus nataliae*, the scapulae meet ventromedially along most of the medial margin to the posteromedial process, forming a dorsoventrally thickened symphysis (Andrews, 1910; Berezin, 2011; O'Keefe and Street, 2009). The posteromedial process of the scapula contacts the anteromedial process of the coracoid along an ovate facet, producing a complete pectoral bar.

Ophthalmothule cryostea bears a short and broad dorsal process of the scapula, in contrast to cryptoclidids from the Oxford Clay, where the extension of the dorsal process can exceed half the total anteroposterior length of the element (Andrews, 1910). This morphology also differs from *Abyssosaurus nataliae* and *Djupedalia engeri*, where the dorsal process forms a large part of the

anterior portion of the element, being both anteroposteriorly extensive and dorsally extended (Berezin, 2011; Knutsen, Druckenmiller and Hurum, 2012a). The glenoid region is dorsoventrally thickened in comparison to the rest of the element and bears a facet for the glenoid and coracoid that are subequal in length, similar to that observed in *Abyssosaurus nataliae* (Berezin, 2011), but differing from that seen *Cryptoclidus eurymerus* and *Djupedalia engeri*, where the coracoid facet is the larger of the two facets (Andrews, 1910; Knutsen, Druckenmiller and Hurum, 2012a) and to *Spitrasaurus wensaasi* where the coracoid facet is significantly smaller (Knutsen, Druckenmiller and Hurum, 2012b) . In PMO 224.248, the glenoid facet is deeply concave, whereas the coracoid facet is nearly flat, but rugose.

Coracoid

Both coracoids are articulated, although somewhat fragmented posteriorly and medially. The coracoids bear a large anteromedial process, which has a slight bifurcation anteriorly, extending further anteriorly than the scapular facet. The anteromedial process forms most of the medial margin of the ovate pectoral fenestrae, differing from *Colymbosaurus megadeirus* and *Abyssosaurus nataliae* where this margin is mainly formed by the scapula (Benson and Bowdler, 2014; Berezin, 2011) and *Tatenectes laramiensis* where both contribute equally (O'Keefe and Street, 2009). The anterior portion of the medial symphysis is dorsoventrally thickened in comparison to the rest of the element, creating a shelf along the anterior margin (posterior from the pectoral fenestra), as in most derived plesiosauroids (Benson and Bowdler, 2014). The ventrally projecting medial symphysis of the coracoids in *Ophthalmothule cryostea* articulate along the medial symphysis so that the ventral margins form an angle close to 180°. In anterior view the dorsal margins are nearly uniform. The almost uniform dorsal surface in PMO 224.248, could be due to dorsoventral compression. This morphology is similar, although less angled than the more dorsolaterally orientated coracoids of *Cryptoclidus eurymerus* (Andrews, 1910; AJR *pers. obs*. NHMUK R2616) and *Colymbosaurus megadeirus* (Benson and Bowdler, 2014; Roberts et al., 2017). The medial symphysis continues posteriorly throughout the preserved medial margin of the coracoid (Fig. 17). The lateral margin of the coracoid is concave and terminates posterolaterally in a distinct posteriorly curved cornu, which just exceeds the lateral margin of the glenoid in the parasagittal plane. The posterior margin is concave and a groove is present medial to the cornu, possibly to articulate with the anterior gastralia.

850 ***Humerus***

851 Both humeri are predominantly uncrushed and well-preserved, except for the tuberosity which is
852 crushed on both (See supplementary information, Table S5 for measurements). In dorsal view, the
853 proximal portion of the humerus is angled slightly anteriorly, resulting in a sigmoidal shape in
854 dorsal view similar to some leptocleidids and polycotylids (Hampe, 2013). Ventrally, a prominent
855 rugosity is present near the proximal end, forming the dorsoventrally thickest point of the humerus
856 (Fig. 18). As in *Djupedalia engeri*, the anteroposterior shortest point is just proximal to the ventral
857 rugosity, after which the humeral shaft gradually distally expands in anteroposterior width
858 (Knutsen, Druckenmiller and Hurum, 2012a). This morphology differs from the more distally
859 constricted morphology observed in *Spitrasaurus*, *Muraenosaurus leedsii*, *Tricleidus seeleyi*,
860 *Pantosaurus striatus* and *Cryptoclidus eurymerus*, where the shaft is anteroposteriorly shortest
861 towards the midshaft and anteroposteriorly expanded at the proximal and distal ends (Andrews,
862 1910; Benson and Bowdler, 2014; Brown, 1981; Knutsen, Druckenmiller and Hurum, 2012b;
863 O'Keefe and Wahl, 2003a). Posteriorly, there are at least three nutritive foramina perforating the
864 posterior surface near the mid-point of the shaft, an uncommon trait in cryptoclidids, but it is also
865 observed in *Spitrasaurus wensaasi* (Knutsen, Druckenmiller and Hurum, 2012b).

866 Distally, there is little to no preaxial expansion. A large, posteriorly expanded postaxial
867 flange is present, although not to the same degree as seen in *Colymbosaurus svalbardensis*
868 (Knutsen, Druckenmiller and Hurum, 2012c; Roberts et al., 2017). PMO 214.248 lacks an
869 anteroposteriorly oriented bisecting ridge on the distal epipodial facets, as observed in some
870 specimens of *Colymbosaurus megadeirus* (Benson and Bowdler, 2014). The distal articular end of
871 the humerus bears three conspicuous convex facets for the radius, ulna and a postaxial accessory
872 element. Along the anterior margin, a rugosity is present, possibly representing a facet for a
873 preaxial accessory element found in articulation on one of the limbs (supplementary information,
874 Fig. S.7). The postaxial flange has at least one facet angled posterodistally, although a secondary
875 postaxial facet could be present directly posteriorly. Whether this posterior-most facet is an actual
876 facet or for connective tissue attachment is equivocal, as no element was found in articulation. The
877 distal facet morphology in *Ophthalmothule cryostea* differs from the two distal facets seen in
878 *Muraenosaurus leedsii* and *Tricleidus seeleyi* (Andrews, 1910), the three seen in *Colymbosaurus*

(a single postaxial ossicle facet; Roberts et al., 2017) and the four seen in '*Plesiosaurus*' *mansellii* (two postaxial facets; Hulke, 1870).

Epipodials and mesopodials

The radius, ulna and postaxial ossicle element are fused through taphonomic processes to one another and likewise the radius is partially fused to the humerus. In addition, the right forelimb preserves an *in situ* oval preaxial element found adjacent to the preaxial facet (supplementary information, Fig. S.8). In proximal view, there is a shallow groove present on the radius and ulna for articulation with the convex distal margin of the humerus. In contrast to the Oxford Clay Formation cryptoclidids with advanced ossification (e.g., *Cryptoclidus eurymerus*; Andrews, 1910; Brown, 1981), an epipodial foramen (*spatium interosseum*) is absent.

The radius is the largest of the epipodial elements, being slightly anteroposteriorly wider and proximodistally longer than the ulna (Fig. 18A). This differs from *Colymbosaurus svalbardensis*, where the radius is proximodistally longer, but anteroposteriorly shorter than the ulna (Roberts et al., 2017) and *Spitrasaurus* spp., *Djupedalia engeri* and *Pantosaurus striatus*, where the radius is at least twice the size of the ulna in all dimensions (Knutsen, Druckenmiller and Hurum, 2012a; b; O'Keefe and Wahl, 2003a). In dorsal view, the outline of the radius has a convex anterior margin which slopes posterodistally, resembling that of *Spitrasaurus larseni* (Knutsen, Druckenmiller and Hurum, 2012b). In proximal view the radius is dorsoventrally thickest posteriorly and thinnest along its anterior margin. The radius has four dorsoventrally thick facets for the humerus, ulna, intermedium, radiale and an anterior facet for a preaxial ossicle (supplementary information, Fig. S.9). The facet for a preaxial accessory element is shared between the anterior margins of the radius and radiale, as described for *Spitrasaurus larseni* (Knutsen, Druckenmiller and Hurum, 2012b). Two small elements, although disarticulated adjacent to the right forelimb along the preaxial margin, could represent part of an anterior accessory row (supplementary information. Fig. S.8).

The ulna is anteroposteriorly wider than proximodistally long, although significantly less than the extremely anteroposteriorly elongated ulna observed in *Colymbosaurus svalbardensis* (Roberts et al., 2017). As in *Pantosaurus striatus* (O'Keefe and Wahl, 2003a), the ulna of *Ophthalmothule cryostea* has five facets, with the largest facet for the humerus, two smaller

anterior and posterior elements for the radius and postaxial ossicle respectively, and two distal facets of subequal size for the intermedium and ulnare.

The postaxial ossicle has three facets for the humerus, ulna and ulnare, and is convex along its posterior margin. As the postaxial element was fused to the ulna, it is possible to reconstruct its position relative to the humerus accurately. Based on this interpretation, the preserved postaxial element, occupies only a small portion of the postaxial margin of the humerus. This is somewhat different from "*Plesiosaurus" mansellii*, where the postaxial elements occupy the entire distal postaxial margin (Hulke, 1870).

The mesopodial elements were partially articulated and identified either by their position relative to the epipodial elements or their morphology. In both forelimbs all the mesopodial elements are preserved. The radiale is the largest of the three and bears five facets; the largest being for the radius, the smallest for the intermedium, two facets for the 1st and 2nd distal carpal and a facet along the anteroproximal margin for a preaxial ossicle. The intermedium bears six facets, two proximal facets for the radius and a longer facet the ulna and three smaller facets for the ulnare, 3rd distal carpal and radiale. The ulnare is bears five facets, two proximal subequal facets for the ulna and postaxial ossicle and three subequal facets for the intermedium, 3rd carpal and 2nd post axial element.

Metacarpals and phalanges

The metacarpals were disarticulated; the distal carpals are small and their articulation to the rest of the limb uncertain. Two of the carpals are proximodistally reduced and rounded in dorsal outline. This morphology differs from the more elongated and angular distal carpals seen in most cryptoclidids (*Colymbosaurus svalbardensis*, *Cryptoclidus eurymerus*, *Muraenosaurus leedsii*, *Tricleidus seeleyi*; Andrews, 1910; Brown, 1981; Roberts et al., 2017). A possible 5th metacarpal was identified based on the unusual morphology of the element and on its proximal position and articulating elements. This element seems to be nearly entirely shifted into the distal carpal row.

Twenty-nine phalanges and/or metacarpals are preserved in the right forelimb and twenty-two in the left. Many of these were removed during excavation, although their location was noted. The proximal phalanges are hourglass-shaped, with flat articular surfaces, whereas the more distal

phalanges, are proximodistally shorter and more compact, similar to that observed in *Colymbosaurus svalbardensis* (Roberts et al., 2017).

Femora

Fragments of the femora from PMO 224.248, were located downslope from the skeleton. These consist of fragments of the distal, mid-shaft and proximal sections of the femur and were identified based on the amount of weathering. The left limb was partly preserved with the rest of the body and was therefore more proximal to the rest of the skeleton and less weathered. The partial femur interpreted as the left, consists of a distal end, shaft fragments and part of the proximal end (supplementary information, Fig. S.10). The bone texture and shape suggests that the femur had a postaxial flange, although not preserved. On the distal fragment of the left femur, part of the distal surface is preserved, which is smooth and slightly convex. When comparing the femoral cross-sections to the complete humeri in PMO 224.248, it is clear that the femora have a smaller circumference than the humeri along the shaft.

Hind limb elements

Distal elements from the left hind limb, including the meso- and metatarsals and several phalanges, are preserved in PMO 224.248 and are partially articulated although heavily weathered (supplementary information, Fig. S.11). Five mesopodial elements are preserved in left hind limb, representing the fibulare, astragalus, tibiale and the two distal tarsal elements. The 5th metatarsal appears to be entirely shifted into the distal tarsal row. Several complete and partial phalanges are preserved. As seen in *Colymbosaurus*, the largest element in dorsal view of the mesopodial elements is the fibulare (Knutsen, Druckenmiller and Hurum, 2012c; Roberts et al., 2017). The fibulare has six facets, with the largest being for the fibula. Along the posterior margin of the fibula there are two facets, one proximally for the postaxial ossicle and another distally possibly for a second ossicle. The astragalus is oval in outline, but bears a proximal convexity, to separate the facets for the fibula and tibia. The element is dorsoventrally thicker than proximodistally long (excluding the proximal surface convexity). The tibiale is the smallest of the three elements and bears five facets, a proximal facet for the tibia, two short proximal facets for the astragalus and second distal tarsal, a long distal facet for the first distal tarsal and a short anterior facet, possibly for a preaxial row. The distal lengths of the tibia and fibula can be estimated, based on the close

articulation between the tibiale, astragalus and fibula. This suggests that at least, the distal anteroposterior extent of the fibula, appears to be longer than that of the tibia. Four metatarsals are preserved, the second, third, fourth and possibly the fifth. As in most cryptoclidids, the forth metatarsal is the largest (Knutsen, Druckenmiller and Hurum, 2012c).

Discussion

Phylogenetic analysis and interrelationships of Cryptoclididae

Ophthalmothule cryostea (PMO 224.248) was scored into the data matrix of Roberts et al., (2017), which is a modification of the matrix from Benson and Druckenmiller (2014). Based on the results of the present study, three new characters (Characters 271-273) were created on features relevant to Cryptoclididae and include two cranial and one post-cranial feature (discussed more fully below). Additional modifications as alternative scoring and information on how to recognise the character states of individual cryptoclidid taxa are available in the supplementary information. Two cranial characters were added, one relating to the presence of an interfrontal vacuity and the other relating to the dorsal surface of the dentary. In addition, a previously used postcranial character relating to the fibular morphology, was edited and included in the matrix. The resulting matrix totals 273 unordered morphological characters and 76 OTUs.

The analysis was performed in TNT (V.1.5) (Goloboff and Catalano, 2016) using the new technology search (Ratchet), combined with Tree bisection reconnection (TBR). The analysis used 1000 iterations, with 10 random addition sequences and 10 random seed. All trees were kept and auto constrain turned off and all characters were equally weighted. *Yunguisaurus* was defined as the outgroup taxon (Cheng et al., 2006). The bremer function in TNT (V 1.5) was used to calculate Bremer support (decay index). Bootstrap resampling (1000 replications), was also performed (supplementary information, Fig. S.5). The scripts stats.run was used to calculate CI and RI. The complete consensus tree for plesiosauromorpha is available in supplementary information (Fig. S.14).

Time scaling was completed in R Studio (Cran) and utilised data collected from PBDB (Palaeontological Database), in addition to personal observations. The *Datephylo* function from the R package *strap* (Bell and Lloyd, 2014), was utilised to form the time scaled tree (See supplementary information for data).

Results of the phylogenetic analysis

The strict consensus tree of 144 MPTs (most parsimonious trees) shows the monophyly of Cryptoclididae is relatively well supported (Fig. 19) with a bremer support of four, as in previous studies (Benson and Bowdler, 2014).

Cryptoclididae is supported by the following seven synapomorphies (character number/state): (144/1) the atlantal centrum participates in the anterior rim of the atlantal cup (state 0 *Tatenectes laramiensis*); 202/0 the anterolateral margin of the scapula is flat/gently convex; (235/1), in the forelimb the digits/tarsal/carpal axis extends posterodistally relative to propodial long axis because proximodistal length of radius/tibia is substantially greater than that of the ulna/fibula; (245/1), the preaxial expansion on the distal margin of the humerus is smaller than the postaxial expansion (2 in *Cryptoclidus eurymerus* and ambiguous between 1&2 in *Spitrasaurus sp.*); (255/3), ratio of tibia length to maximum width is >0.75 (state 1 in *Pantosaurus striatus* and state 2 in *Colymbosaurus megadeirus*); (261/2), an epipodial foramen is absent (state 0 in *Muraenosaurus leedsii*, 1 in '*Picrocleidus' beloclis* and *Tricleidus seeleyi,* 1&2 in *Cryptoclidus eurymerus* depending on ontogeny, ambiguous in *Abyssosaurus laramiensis*); (262/1), the ratio of maximum radius length to maximum ulna length is between 1.4-1.7 (state 0 in *Ophthalmothule cryostea*, state 2 in *Cryptoclidus eurymerus*). It is noteworthy that all of these synapomorphies are postcranial features, due to the lack of complete and/or well-preserved cranial material in this clade. In the analysis of Benson and Bowdler (2014) only one of these characters (144) was recovered as a synapomorphy in their diagnosis. *Ophthalmothule cryostea* can be referred to the family Cryptoclididae on the basis of sharing three of seven synapomorphies (two could not be scored for *Ophthalmothule cryostea*).

As found in Benson and Bowdler (2014), Cryptoclididae is split into two subclades, one of which has been formally named as Colymbosaurinae. In Benson and Bowdler (2014), this subfamily includes *Colymbosaurus*, *Spitrasaurus*, *Djupedalia engeri*, *Pantosaurus striatus*, *"Plesiosaurus" mansellii* and *Abyssosaurus nataliae*. As cranial material for these taxa is either limited or unavailable, the synapomorphies include only post-cranial features. This is problematic, as there could be a conflicting signal between cranial and post-cranial characters in the data matrix. PMO 224.248 could be scored for a significant number of cranial and post cranial characters in the matrix. Although not recovered in the subfamily, *Ophthalmothule cryostea* shares three of the

five Colymbosaurinae synapomorphies described in Benson and Bowdler (2014). The addition of this new taxon to the data set, along with the three new characters, created a new topology for the cryptoclidid clade. Although the two major subclades are still present, the Slottsmøya Member taxa *Spitrasaurus spp.*, *Djupedalia engeri* and *O. cryostea* were removed from the Colymbosaurinae subfamily and placed as a sister group to *Cryptoclidus eurymerus*, *Tatenectes laramiensis* and *Kimmerosaurus langhami*. Although this configuration is supported with higher Bremer support values than those reported in Benson and Bowdler (2014), most of the internal structure of the cryptoclidid tree was not retained after running a resampling bootstrap analysis and all nodes received low support (≥50). However, this analysis does show that a revision is required of the diagnostic features of Colymbosaurinae in light of the new taxon (PMO 224.248). As a result, four synapomorphies for the reduced Colymbosaurinae clade were recovered: (197/0) the anteromedial margin of the coracoid does not contact the scapula; (209/2), the coracoid anteromedial process is short and subtriangular; (224/1), the anteroposterior width of the ilium is expanded, between 1.5-2.0 times the minimum anteroposterior width of the shaft and (256/1), the anterior margin of the radius is straight or convex.

Although the precise position of *Ophthalmothule cryostea* (PMO 224.248) as sister taxon to *Spitrasaurus* spp. is weakly supported (Bremer Support =2), the clade incorporating *Djupedalia engeri*, *Spitrasaurus* spp. and *O. cryostea* receives higher support (Bremer Support = 3). This clade ~~is~~ shares three synapomorphies: (152/5) the number of cervical vertebrae is between 50-60; (157/2) the anterior cervical neural spines are inflected anterodorsally (ambiguous in PMO 224.248) and (234/1), the presence of preaxial ossicles. The separation of this Slottsmøya Member restricted clade from Colymbosaurinae, suggests that at least two separate clades of cryptoclidids were present in the Boreal region during the Late Jurassic – Early Cretaceous.

Palaeobiological implications

Cranial morphology and feeding ecology

The skull of *Ophthalmothule cryostea* displays relatively large orbits compared to the temporal fenestrae (both measured as anteroposterior length; = ~1.7) in comparison with other cryptoclidid taxa for which this can be measured (*Cryptoclidus eurymerus*, ~0.93; *Muraenosaurus leedsii*, ~0.58). However, a comparison of orbit versus total skull length in PMO 224.248 (= 0.29), is closer, but still significantly different to that of other cryptoclidid plesiosaurs (*Cryptoclidus*

eurymerus, ~0.21; *Muraenosaurus leedsii*, ~0.17). When compared to estimated body length (skull length/estimated body length), the skull of PMO 224.248 is considerably smaller compared to the published body size estimates in other cryptoclidids (Brown, 1981). In *Ophthalmothule cryostea* (PMO 224.248), the skull represents an estimated 4% of total estimated body length (5-5.5m), while in *Muraenosaurus leedsii* specimen NHMUK R.2422, the skull is estimated to constitute 7-8 % of the total body length (see supplementary information 3).

The mediolateral expansion of the dorsal surface of the mandible, displays an almost lateral exit angle for the teeth from the alveoli in *Ophthalmothule cryostea* and is extremely similar to the morphology seen in *Spitrasaurus larseni* (Knutsen, Druckenmiller and Hurum, 2012b). In *Ophthalmothule cryostea* the maximum cross-sectional diameter of one of the crowns (at crown-root transition) is ~5.5 mm and is somewhat larger to that described for *Kimmerosaurus langhami* and *S. larseni* (<5 mm; Brown, 1981; Knutsen, Druckenmiller and Hurum, 2012b). Some of the teeth of PMO 224.248 show wear facets, indicating a tight fit between the lower and upper jaw teeth. This differs from the teeth described for *K. langhami*, where no abrasion or wear is visible on the crowns (Brown, 1981). The preserved teeth of *O. cryostea* are not as recurved as those in *S. larseni* and *K. langhami*, and therefore probably displayed a more protruding dentition than these taxa. Based on their phylogenetic position in the plesiosaurian tree, a similar morphology evolved independently in the elasmosaurid *Aristonectes parvidens* (Gasparini et al., 2003). However, the morphology is *A. parvidens* is more extreme as the alveoli face directly laterally in the mandible (Gasparini et al., 2003).

Calculations of mechanical advantage can be used to suggest the strength of the jaw in reptiles (Stubbs et al., 2013; Foffa, 2018). Two calculations of mechanical advantage were completed on different cryptoclidid taxa (See supplementary information 3 for methodology and measurements), anterior mechanical advantage (AMA) and posterior mechanical advantage (PMA). The mechanical advantage of the jaw of *Ophthalmothule cryostea* was estimated to be 0.13/0.44 (AMA/PMA). This numbers are low, illustrating a low mechanical advantage, similar to *Kimmerosaurus langhami* (0.13/0.51) and *Spitrasaurus larseni* (0.11/0.31). In comparison the mechanical advantage calculated was somewhat higher in Callovian cryptoclidids: *Cryptoclidus eurymerus* (PETMG R283: 0.19/0.73), *Muraenosaurus leedsi* (NHMUK R2422: 0.20/0.64) and *Tricleidus seeleyi* (NHMUK R3539: 0.18/0.72). The mechanical advantage of these cryptoclidids

is generally lower than those calculated for larger macro predatory marine reptiles (Stubbs et al., 2013). This suggests, particularly in the case of *O. cryostea* and *Spitrasaurus*, that these marine reptiles had a low bite force and would have been unable to eat larger, more armoured prey as suggested by tooth morphology.

In vertebrates, the ~~orbital~~ size, which is limited by absolute constraints, cannot be reduced in size without impacting visual ability. Enlarged eyes accommodates additional photoreceptive cells and has additional area for light intake, thereby increasing the capability of the animal to see in low-light conditions (e.g.deep, murky water, at night or during darker seasons; Motani, Rothschild and Wahl, 1999; Fernández et al., 2007). *Ophthalmothule* was present in a northern, although not Arctic region and would have experienced seasonality (Galloway et al., 2013). This alone may have been the purpose for higher visual acuity, or may have been in addition to deep-diving (Berezin, 2018). Enlarged orbits in comparison to the temporal region are also described for the Cretaceous sub-Boreal Russian cryptoclidid *Abyssosaurus nataliae* (Berezin, 2018). In *A. nataliae* this morphology is suggested to be a paedomorphic feature; a retention of large orbits and short temporal region is a common juvenile feature in reptiles, including marine reptiles (Johnson, 1977). Phylogenetically, *A. nataliae* and *Ophthalmothule cryostea* are in two separate clades of cryptoclidids. Although this feature may not be paedomorphic, it does suggest that a high orbital/cranial ratio is present in at least two lineages of Late Jurassic - Early Cretaceous cryptoclidids.

In conclusion, to accommodate high visual acuity in the small cranium of *Ophthalmothule cryostea*, pressure to reduce the size of other areas of the cranium such as the temporal region may have been increased. However, a more likely scenario is that this odd adaptation is a result of dietary selection. In *O. cryostea*, this gracile and trap-like dentition in combination with the enlarged orbit relative to temporal fenestral size and low mechanical advantage, suggests that *O. cryostea* may have fed on small, "soft-bodied" prey from the water column or sea floor and the large orbital size may have increased visual acuity in these environments (Fig. 20) (Massare, 1987; Noè, Taylor and Gómez-Pérez, 2017).

Complex evolution of neck length and flexibility in plesiosauroids

Despite sharing the same plesiosauroid body form, cryptoclidids display high disparity in the number and morphology of the cervical vertebrae between genera. Noè, Taylor and Gómez-Pérez

(2017), used three taxa of cryptoclidid plesiosaurs (*Muraenosaurus*, *Tricleidus* and *Cryptoclidus*), to illustrate neck flexibility and function, although did not provide any quantitative analysis. For elasmosaurids, the number of cervical vertebrae has been demonstrated to have had multiple independent reductions over time (Serratos, Druckenmiller and Benson, 2017), contra to previous research (Sachs, Kear and Everhart, 2013). Although the number of cervical vertebrae is unknown for a significant fraction of Late Jurassic – Early Cretaceous cryptoclidid taxa, *Ophthalmothule cryostea* and the Slottsmøya Member genera *Spitrasaurus* and *Djupedalia*, have an increased number of cervicals (character 152/5-6) in comparison to the ancestral state in cryptoclidids (152/3-4). Based on the available specimens, the number of cervical vertebrae appears to have generally increased over time at least in one clade of cryptoclidids, with the highest number recorded in the Slottsmøya Member (Upper Jurassic) taxon *Spitrasaurus wensaasi* (60: Knutsen, Druckenmiller and Hurum, 2012b). Although a high cervical count may be the case for the Slottsmøya plesiosauroids, more evidence is required. We suggest that a study focusing on number of cervicals and flexibility be completed.

Conclusion

Ophthalmothule cryostea (PMO 224.248) represents the temporally youngest occurrence of a plesiosaur from the Slottsmøya Member (Agardhfjellet Formation) of central Spitsbergen. *O. cryostea* represents the forth taxon described from the member, although several other cryptoclidid specimens remain to be described. *O. cryostea* is one of the few cryptoclidids with detailed cranial osteology available, providing much needed morphological information for understanding the intrarelationships of cryptoclidids. In addition, this specimen uniquely preserves a complete cervical series found in articulation, offering future opportunities to test current hypotheses on plesiosaur neck-flexibility and evolution. As the specimen was found in the section encompassing the Jurassic – Cretaceous boundary and likely Berriasian in age, PMO 224.248 along with the Russian *Abyssosaurus nataliae* represent the only cryptoclidid genera that cross the Jurassic – Cretaceous boundary. The phylogenetic results of this study indicate that two separate clades of cryptoclidids crossed the Jurassic – Cretaceous boundary in the Boreal region of Spitsbergen and the sub-Boreal region of Russia.

Acknowledgements

The authors wish to thank the museum curators and researchers that assisted AJR during collection visits; S. Chapman and L. Steel (NHMUK), M. Riley (CAMSM), E. Howlett (OUM), M. Evans (LEICS), M. Fernández (MOZ, MLP), G. Wass (PETMG), N. Clark (GLAHM), G. Cuny (MGUH), K. Sherburn (MANCH), L. A. Vietti (UW). D. Foffa, S. Etches, V. E. Nash, D. Legg, A. S. Smith, V. Fischer, J. Wujek, E. M. Knutsen and E. Martin-Silverstone are thanked for discussion. M-L K. Funke, C. Ekeheien, M. Koevoets and V. E. Nash are thanked for assistance during the preparation of the specimen. Ø. Hammer is thanked for assistance with the computed tomography and O. Katsamensis is thanked for access to the visualisation laboratory (μ-vis) in Southampton. M. J. Benton is thanked for comments on an earlier version of the manuscript. The Willi Hennig Society is acknowledged for their sponsorship of TNT (Trees with New Technology). Gratitude is warranted to all the volunteers of the Spitsbergen Mesozoic Research Group, who participated in the 2012 excavations during their holidays. The authors warmly thank the palaeoartist Esther van Hulsen for illustrating PMO 224.248.

References

Andrews CW. 1910. *A descriptive catalogue of the Marine Reptiles of The Oxford Clay Based on the Leeds Collection in the British Museum (Natural History).* British Museum (Natural History), London. 205 pp.+x plates

Bell, MA, Lloyd, GT. 2014 strap: an R package for plotting phylogenies against stratigraphy and assessing their stratigraphic congruence. *Palaeontology* **58**:379-389.

Benson RBJ, Bowdler T. 2014. Anatomy of Colymbosaurus megadeirus (Reptilia, Plesiosauria) from the Kimmeridge Clay Formation of the U.K., and high diversity amoung Late Jurassic plesiosauroids. *Journal of Vertebrate Paleontology* **34**:1053 – 1071.

Benson RBJ, Evans M, Druckenmiller PS. 2012. High Diversity, Low Disparity and Small Body Size in Plesiosaurs (Reptilia, Sauropterygia) from the Triassic–Jurassic Boundary. *PLOS ONE* **7**:e31838.

Benson RBJ, Druckenmiller PS. 2014. Faunal turnover of marine tetrapods of the Jurassic–Cretaceous transition. *Biological Reviews* **89**:1–23.

Berezin AY. 2011. A New Plesiosaur of the Family Aristonectidae from the Early Cretaceous of the Center of the Russian Platform. *Paleontological Journal* **45**:648–660.

Berezin AY. 2018. Craniology of the plesiosaur *Abyssosaurus natalie* Berezin (Sauropterygia, Plesiosauria) from the Lower Cretaceous of the Central Russian Platform. *Paleontological Journal* **52**:328–341.

Brown DS. 1981. The English Upper Jurassic Plesiosauridae (Reptilia) and a review of the phylogeny and classification of the Plesiosauia. Bulletin of the British Museum (Natural History), *Geology* **35**:253–347.

Brown DS, Milner AC, Taylor MA. 1986. New material of the plesiosaur *Kimmerosaurus langhami* Brown from the Kimmeridge Clay of Dorset. *Bulletin of the British Museum (Natural History), Geology Series* **40**:225–234.

Brown DS, Cruickshank ARI. 1994. The skull of a Callovian plesiosaur *Cryptoclidus eurymerus*, and the sauropterygian cheek. *Palaeontology* **37**:941–953.

Buchy M-C, Frey E, Salisbury SW. 2006. The internal cranial anatomy of the Plesiosauria (Reptilia, Sauropterygia): evidence for a functional secondary palate. *Lethaia* **39**:289–303.

1189 Carpenter K. 1996. A review of short–necked plesiosaurs from the Cretaceous of the western
1190 interior, North America. Neues Jahrbuch für Geologie und Paläontologie. Abhandlungen
1191 **201**:259p.
1192 Cheng Y-N Sato T, Wu X-C, Li C. 2006. First complete pistosauroid from the Triassic of China.
1193 *Journal of Vertebrate Paleontology* **26**:501-504
1194 Cicimurri DJ, Everhart MJ. 2001. An elasmosaur with stomach contents and gastroliths from the
1195 Pierre Shale (Late Cretaceous) of Kansas. *Transactions of the Kansas Academy of*
1196 *Science* **104**:129–143.
1197 Collignon M, Hammer Ø. 2012. Petrography and sedimentology of the Slottsmøya Member at
1198 Janusfjellet, central Spitsbergen. *Norwegian Journal of Geology* **92**:89–101.
1199 Druckenmiller, PS. 2002. Osteology of a new plesiosaur from the Lower Cretaceous (Albian)
1200 Thermopolis Shale of Montana. *Journal of Vertebrate Paleontology* **22**:29–42.
1201 Druckenmiller PS, Hurum JH, Knutsen EM, Nakrem HA. 2012. Two new ophthalmosaurids
1202 (Reptilia: Ichthyosauria) from the Agardhfjellet Formation (Late Jurassic:
1203 Volgian/Tithonian), Svalbard, Norway. *Norwegian Journal of Geology* **92**:311–339.
1204 Dypvik H, Nagy J, Eikeland TA, Backer-Owe K, Andresen A, Johansen K, Elverhoi A, Haremo
1205 P, Bjaerke T. 1991. The Janusfjellet Sugroup (Bathonian to Hauterivian) on central
1206 Spitsbergen: a revised lithostratigraphy. *Polar Research* **9**:21–43.
1207 Everhart MJ. 2000. Gastroliths associated with plesiosaur remains in the Sharon Springs Member
1208 of the Pierre Shale (Lat Cretaceous), Western Kansas. *Transactions of the Kansas*
1209 *Academy of Science* **103**:64–75.
1210 Fernández MS, Arcguby F, Talevi M, Evner R. 2005. Ichthyosaurian eyes: paleobiological
1211 information content in the sclerotic ring of *Caypullisaurus* (Ichthyosauria,
1212 Ophthalmosauria). *Journal of Vertebrate Paleontology* **25**:330–337.
1213 Foffa, D. 2018. The ecology and evolution of the marine reptile faunas of the Jrassic sub-Boreal
1214 Seaway. PhD thesis. The University of Edinburgh. Edinburgh. United Kingdom.
1215 Galloway JM, Sweet AR, Swindles GT, Dewing K, Hadlari T, Embry AF, Sanei H. 2013.
1216 Middle Jurassic to Lower Cretaceous paleoclimate of Sverdrup Basin, Canadian Arctic
1217 Archipelago inferred from the palynostratigraphy. *Marine and Petroleum Geology*
1218 **44**:240-255.

1219 Gasparini Z, Bardet N, Iturralde-Vincent M. 2002. A new cryptoclidid Plesiosaur from the
1220 Oxfordian (Late Jurassic) of Cuba. *Geobios* **35**:201–211.
1221 Gasparini Z, Bardet N, Martin JE, Fernández MS. 2003. The elasmosaurid plesiosaur
1222 Aristonectes Cabrera from the latest Cretaceous of South America and Antarctica.
1223 *Journal of Vertebrate Paleontology* **23**:104–115.
1224 Goloboff PA, Catalano SA. 2016. TNT version 1.5, including a full implementation of
1225 phylogenetic morphometrics. *Cladistics* **32**:221–238.
1226 Hammer Ø, Collignon M, Nakrem HA. 2012. Organic carbon isotope chemostratigraphy and
1227 cyclostratigraphy in the Volgian of Svalbard. *Norwegian Journal of Geology* **92**:103–
1228 112.
1229 Hampe O. 2013. The forgotten remains of a leptocleidid plesiosaur (Sauropterygia:
1230 Plesiosauroidea) from the Early Cretaceous of Gronau (Mu¨nsterland, Westphalia,
1231 Germany). *Paläontologisches Zeitschrift* **87**:473–491.
1232 Hryniewicz K, Hammer Ø, Nakrem HA, Little CTS. 2012. Microfacies of the Volgian–
1233 Ryazanian (Jurassic–Cretaceous) hydrocarbon seep carbonates from Sassenfjorden,
1234 central Spitsbergen, Svalbard. *Norwegian Journal of Geology* **92**:113–131.
1235 Hulke JW. 1870. Note on some Plesiosaurian Remains obtained by J. C. Mansel Esq. F.G.S., in
1236 Kimmeridge Bay, Dorset. *Quarterly Journal of the Geological Society of London*
1237 **26**:611–622.
1238 Johnson R. 1977. Size independent criteria for estimating relative age and relationships among
1239 growth parameters in a group of fossil reptiles (Reptilia-ichthyosauria). *Canadian*
1240 *Journal of Earth Sciences* **14**:1916-1924.
1241 Kear BP. 2006. Plesiosaur remains from Cretaceous high-latitude non-marine deposits in
1242 Southeastern Australia. *Journal of Vertebrate Paleontology* **26**:196–199.
1243 Knutsen EM, Druckenmiller PS, Hurum JH. 2012a. A new plesiosaurid (Reptilia–Sauropterygia)
1244 from the Agardhfjellet Formation (Middle Volgian) of central Spitsbergen, Norway.
1245 *Norwegian Journal of Geology* **92**:213–234.
1246 Knutsen EM, Druckenmiller PS, Hurum JH. 2012b. Two new species of long-necked
1247 plesiosaurians (Reptilia–Sauropterygia) from the Upper Jurassic (Middle Volgian)
1248 Agardhfjellet Formation of central Spitsbergen. *Norwegian Journal of Geology* **92**:187–
1249 212.

1250 Knutsen EM, Druckenmiller PS, Hurum JH. 2012c. Redescription and taxonomic clarfication of
1251 '*Tricleidus' svalbardensis* based on new material from the Agardhfjellet Formation
1252 (Middle Volgian). *Norwegian Journal of Geology* **92**:175–186.
1253 Massare JA. 1987. Tooth morphology and prey preference of Mesozoic marine reptiles. *Journal*
1254 *of Vertebrate Paleontology* **7**:121–137.
1255 Motani R, Rothschild BM, Wahl W. 1999. Large eyes in deep diving ichthyosaurs. *Nature*
1256 **402**:747.
1257 McHenry CR, Cook AG, Wroe S. 2005. Bottom-feeding plesiosaurs. *Science* **310**:75.
1258 Noè LL, Taylor MA, Gómez-Pérez M. 2017. An integrated approch to understanding the role of
1259 the long neck in plesiosaurs. *Acta Palaeontologica Polonica* **62**:137–162.
1260 O'Keefe FR. 2001. A cladistic analysis and taxonomic revision of the Plesiosauria (Reptilia:
1261 Sauropterygia). *Acta Zoologica Fennica* **214**:1–63.
1262 O'Keefe FR, Street HP. 2009. Osteology of the cryptocleidoid plesiosaur *Tatenectes laramiensis*,
1263 with comments on the taxonomic status of the Cimoliasauridae. *Journal of Vertebrate*
1264 *Paleontology* **29**:48–57.
1265 O'Keefe FR, Street HP, Wilhelm CDR, Zhu H. 2011. A new skeleton of the cryptoclidid
1266 plesiosaur *Tatenectes laramiensis* reveals a novel body shape among plesiosaurs. *Journal*
1267 *of Vertebrate Paleontology* **31**:330–339.
1268 O'Keefe FR, Wahl W. 2003a. Current taxonomic status of the plesiosaur *Pantosaurus striatus*
1269 from the Upper Jurassic Sundance Formation, Wyoming. *Paludicola* **4**:37–46.
1270 Roberts AJ, Druckenmiller PS, Delsett LL, Hurum JH. 2017. Osteology and relationships of
1271 Colymbosaurus Seeley, 1874, based on new material of C. svalbardensis from the
1272 Slottsmøya Member, Agardhfjellet Formation of central Spitsbergen. *Journal of*
1273 *Vertebrate Paleontology* **37**:e1278381.
1274 Sachs S, Hornung JJ, Kear BP. 2016. Reappraisal of Europe's most complete Early Cretaceous
1275 plesiosaurian: Brancasaurus brancai Wegner, 1914 from the "Wealden facies" of
1276 Germany. *PeerJ* **4**:e2813.
1277 Sachs S, Kear BP, Everhart MJ. 2013. Revised Vertebral Count in the "Longest–Necked
1278 Vertebrate" *Elasmosaurus platyurus* Cope 1868, and Clarification of the Cervical–Dorsal
1279 Transition in Plesiosauria. *PLOS ONE* **8**:e70877.

1280 Sato T, Hasegawa Y, Manabe M. 2006. A new elasmosaurid plesiosaur from the Upper
1281 Cretaceous of Fukushima, Japan. *Palaeontology* **49**:467–484.
1282 Serratos DJ, Druckenmiller PD, Benson RBJ. 2017. A new elasmosaurid (Sauropterygia,
1283 Plesiosauria) from the Bearpaw Shale (Late Cretaceous, Maastrichtian) of Montana
1284 demonstrates multiple evolutionary reductions of neck length within Elasmosauridae.
1285 *Journal of Vertebrate Paleontology*:10.1080/02724634.2017.1278608.
1286 Smith AS. 2007. The back-to-front plesiosaur *Cryptoclidus* (*Apractocleidus*) aldingeri from the
1287 Kimmeridgian of Milne Land, Greenland. *Bulletin of the Geological Society of Denmark*
1288 **55**:1–7.
1289 Smith AS, Benson RBJ. 2014. Osteology of *Rhomaleosaurus thorntoni* (Sauropterygia:
1290 Rhomaleosauridae) from the Lower Jurassic (Toarcian) of Northamptonshire, England.
1291 *Monograph of the Palaeontographical Society* **168**:40pp, 35 pls.
1292 Stubbs, TL, Pierce, SE, Rayfield, EJ, Anderson PSL. 2013. Morphological and
1293 biomechanicaldispariy of crocodile-line archosaurs following the end-Triassic extinction.
1294 *Proceedings of the Royal Society B* **280**:20131940
1295 Taylor, M. P., and M. J. Wedel. 2013. The effect of intervertebral cartilage on neutral posture
1296 and range of motion in the necks of sauropod dinosaurs. *PLOS ONE* **8**:e78214.
1297 Tennant JP, Mannion PD, Upchurch P. 2016. Sea level regulated tetrapod diversity dynamics
1298 through the Jurassic/Cretaceous interval. *Nature Communications* **7**:12737
1299 Vincent P, Benson RBJ. 2012. *Anningsaura*, a basal plesiosaurian (Reptilia, Plesiosauria) from
1300 the Lower Jurassic of Lyme Regis, United Kngdom. *Journal of Vertebrate Paleontology*
1301 **32**:1049–1063.
1302

Figure 1

Map of locality and stratigraphy of the Upper Jurassic (middle Volgian) to the Early Cretaceous part of the Slottsmøya member of the Agardhfjellet Formation (the lowest unit not included, see text) with described cryptoclidid positions.

(A) Geological map of the field site in central Spitsbergen. The arrow points to the excavation site of PMO 224.248 (Modified from Dallmann et al., 2001 and Hurum et al., 2012). Scale bar equals 1 km. (B) The stratigraphic position of PMO 224.248 (in bold) in relation to the other described cryptoclidids specimens (PMO 219.718 – *Spitrasaurus wensaasi*; PMO 222.663, PMO 216.838 – *Colymbosaurus svalbardensis*; PMO 216.839 – *Djupedalia engeri*; SVB 1450 – *Spitrasaurus larseni*). Note the uncertain position of the Jurassic – Cretaceous boundary. Modified from Delsett et al. 2015).

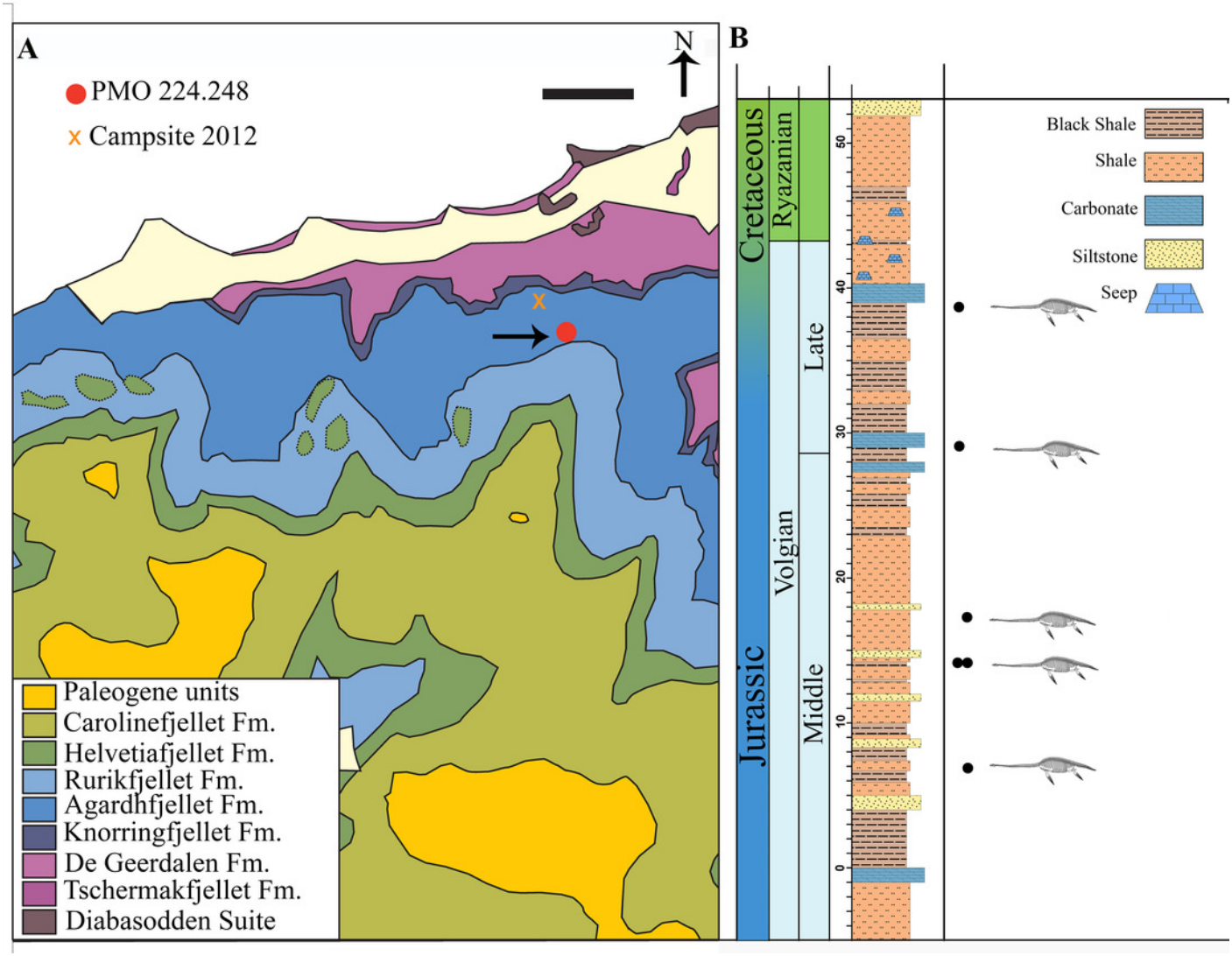
A
N
PMO 224.248
Campsite 2012
Paleogene units
Carolinefjellet Fm.
Helvetiafjellet Fm.
Rurikfjellet Fm.
Agardhfjellet Fm.
Knorringfjellet Fm.
De Geerdalen Fm.
Tschermakfjellet Fm.
Diabasodden Suite
B
Cretaceous
Ryazanian
Jurassic
Volgian
Late
Middle
0
10
20
30
40
50
Black Shale
Shale
Carbonate
Siltstone
Seep

Figure 2

Quarry map and reconstruction of PMO 224.248.

(A) drawing from a combination of field and laboratory drawings in ventral view (modified from Delsett et al., 2016); (B) skeletal reconstruction of PMO 224.248, where red indicates preserved elements. Scale bar equals 50 cm.

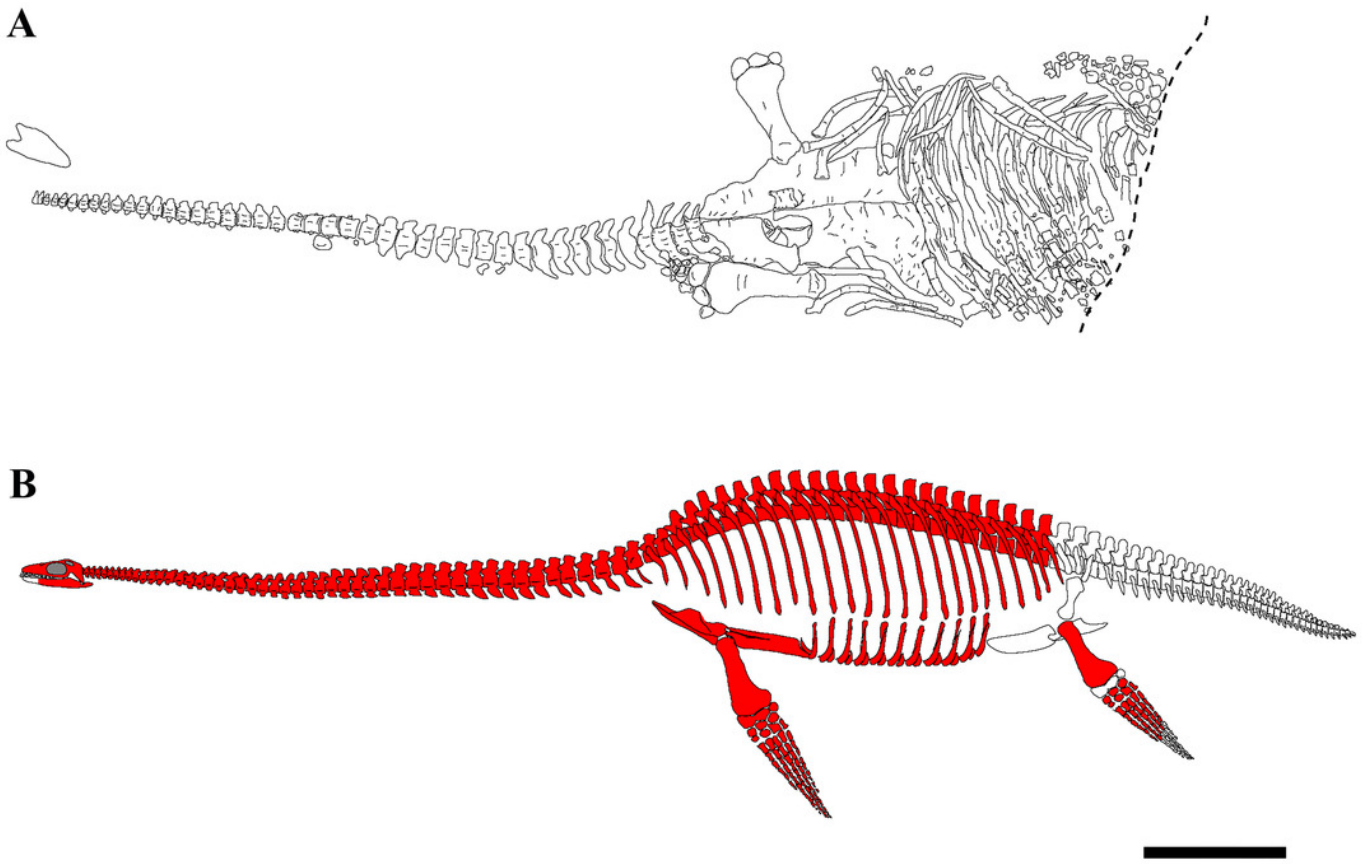

Figure 3

The cranium of *Ophthalmothule* cryostea*,* PMO 224.248 in dorsal view.

(A) photo of PMO 224.248, (B) µCT reconstruction and (C) interpretation. Abbreviations: bo, basioccipital; en, external naris; ex-op, exoccipital-opisthotic; f, frontal; ifv, interfrontal vacuity; mx, maxilla; p, parietal; pif, pineal foramen; pm, premaxilla; pop, paraoccipital process; q, quadrate; so, supraoccipitial; sq, squamosal; tfen, temporal fenestra. Scale bar equals 5 cm. Photograph by Aubrey Roberts

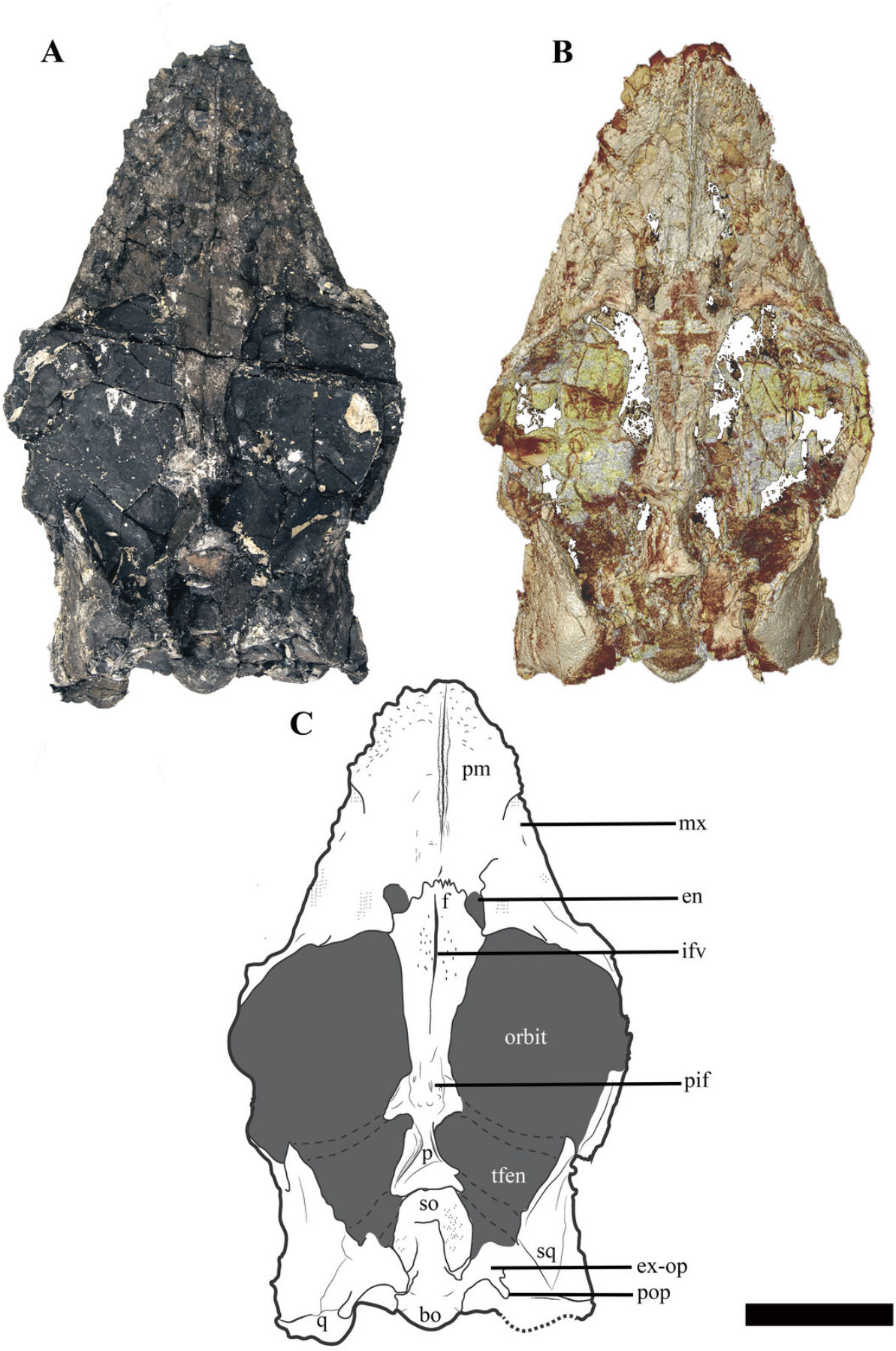
A
B
C
pm
mx
f
en
ifv
orbit
pif
p
tfen
so
sq
ex-op
pop
q
bo

Figure 4

The cranium of *Ophthalmothule cryostea,* PMO 224.248 in palatal view.

(A) photo, (B) µCT reconstruction and (C) interpretation. Abbreviations: aiv, anterior interpterygoid vacuity; bo, basioccipital; in, internal naris; mx, maxilla; pal, palatine; pbs, parabasisphenoid pitf, pituitary fossa; piv, posterior interpterygoid vacuity; pm, premaxilla; pt, pterygoid; q, quadrate; sq, squamosal; stfen, subtemporal fenestra; v, vomer. Scale bar equals 5 cm. Photograph by Aubrey Roberts

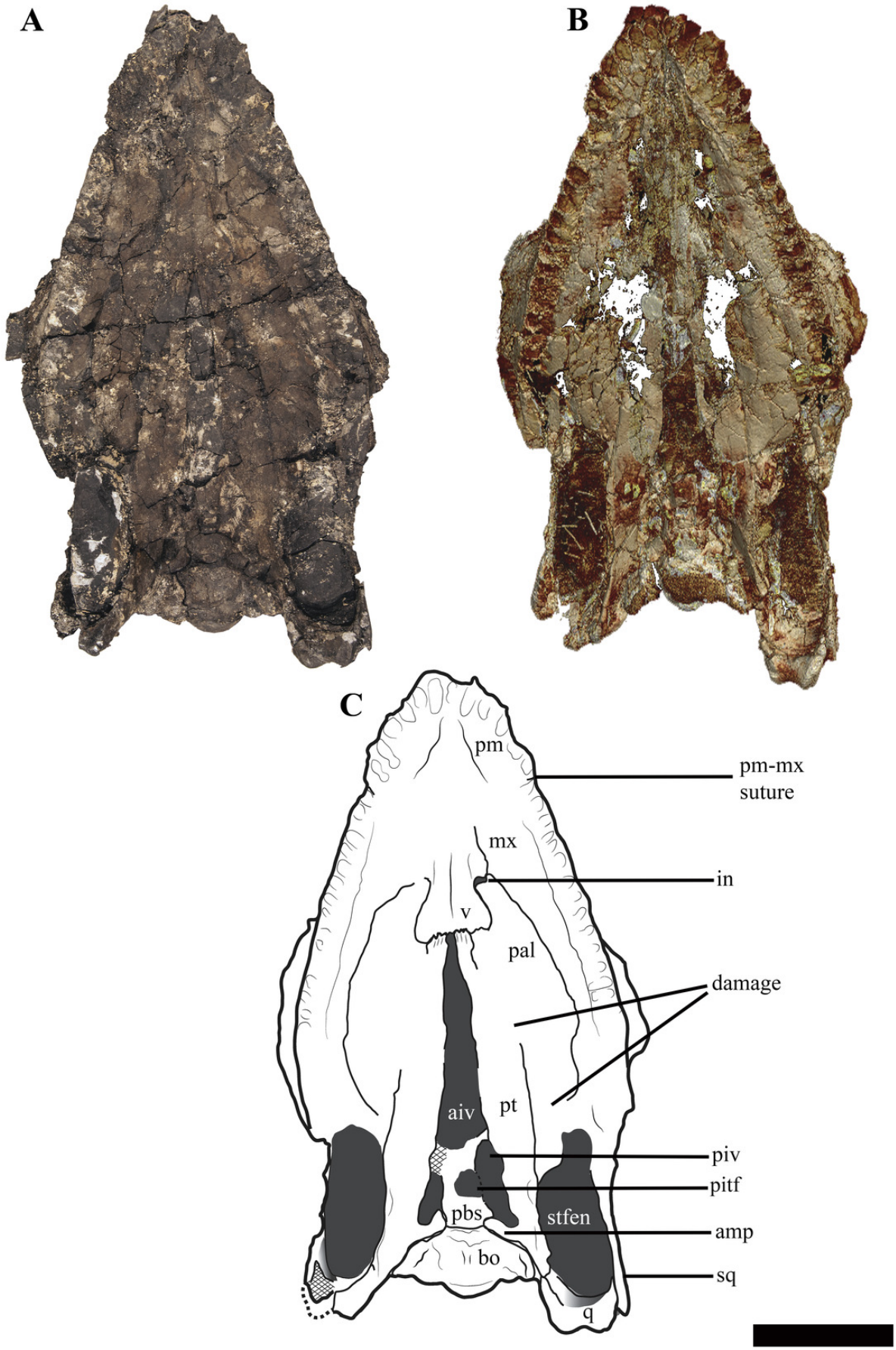
A
B
C
pm
pm-mx
suture
mx
in
v
pal
damage
aiv
pt
piv
pitf
pbs
stfen
amp
bo
sq
q

Figure 5(on next page)

Reconstructions of the cranium of *Ophthalmothule cryostea,* PMO 224.248.

(A) dorsal, (B) palatal and (C) posterior views. Abbreviations: aiv, anterior interpterygoid vacuity; ba, basal articulation; bo, basioccipital; boc, basioccipital condyle; bot, basioccipital tuber; en, external naris; ex-op, exoccipital-opisthotic; f, frontal; ifv, interfrontal vacuity; in, internal naris; mx, maxilla; p, parietal; pal, palatine; pbs, parabasispenoid; pif, pineal foramen; pitf, pituitary fossa; piv, posterior interpterygoid vacuity; pm, premaxilla; pt, pterygoid; q, quadrate; so, supraoccipital; sq, squamosal; stfen, subtemporal fenestra; tfen, temporal fenestra; v, vomer. Scale bar equals 5 cm.

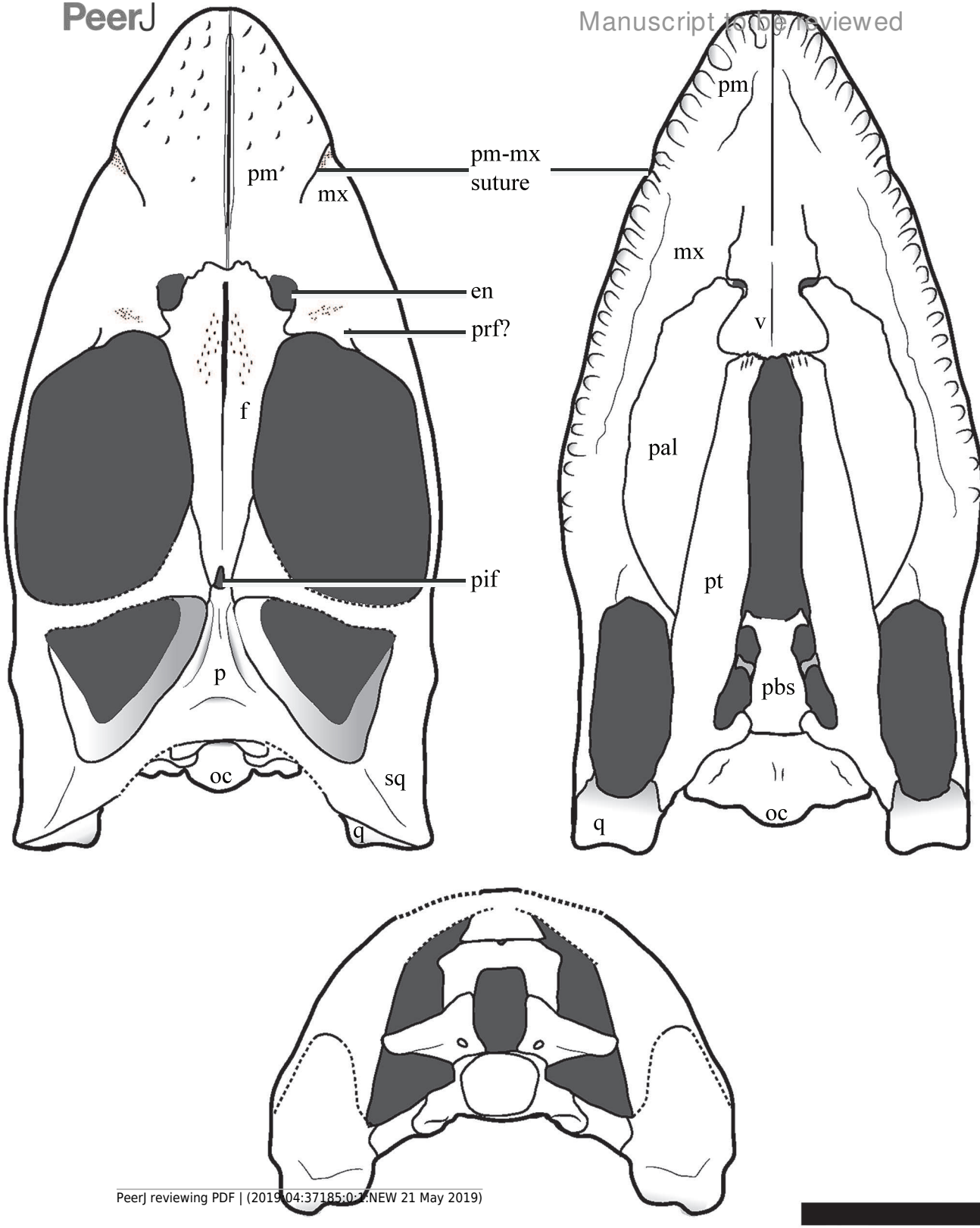

Figure 6

A µCT slice (cross section) of the posterior part of the skull roof and braincase of *Ophthalmothule cryostea,* PMO 224.248, illustrating the parietal fossae and pineal foramen.

Abbreviations: bo, basioccipital; f, frontal; p, parietal; pfos, parietal fossae; pif, pineal foramen; pop, paraoccipital process. Scale bar equals 1 cm.

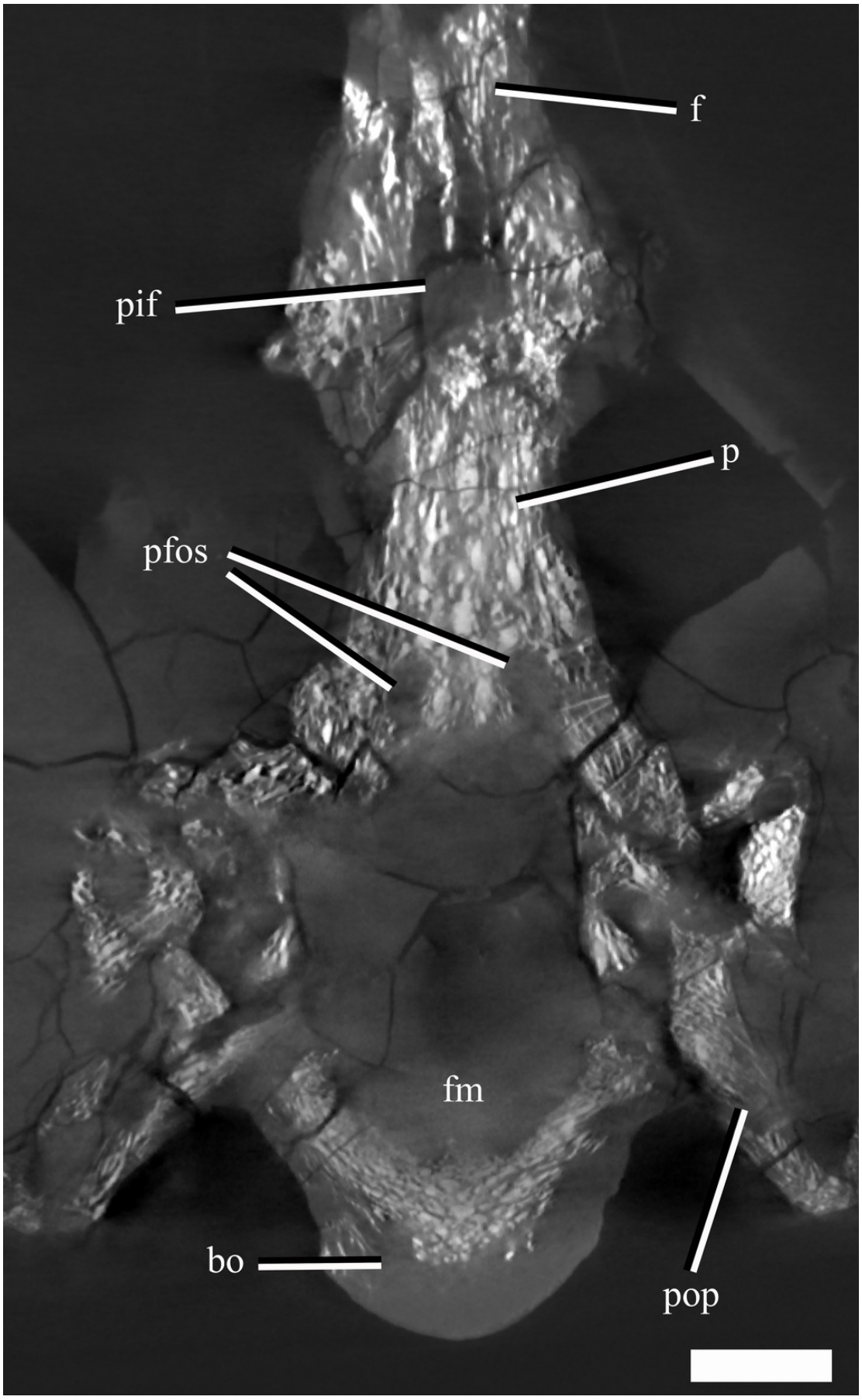
f
pif
p
pfos
fm
bo
pop

Figure 7

The cranium of *Ophthalmothule cryostea,* PMO 224.248 in posterior view.

Abbreviations: boc, basioccipital condyle; ex-op, exoccipital opisthotic; q, quadrate; sq, squamosal. Scale bar equals 1 cm. Photograph by Aubrey Roberts

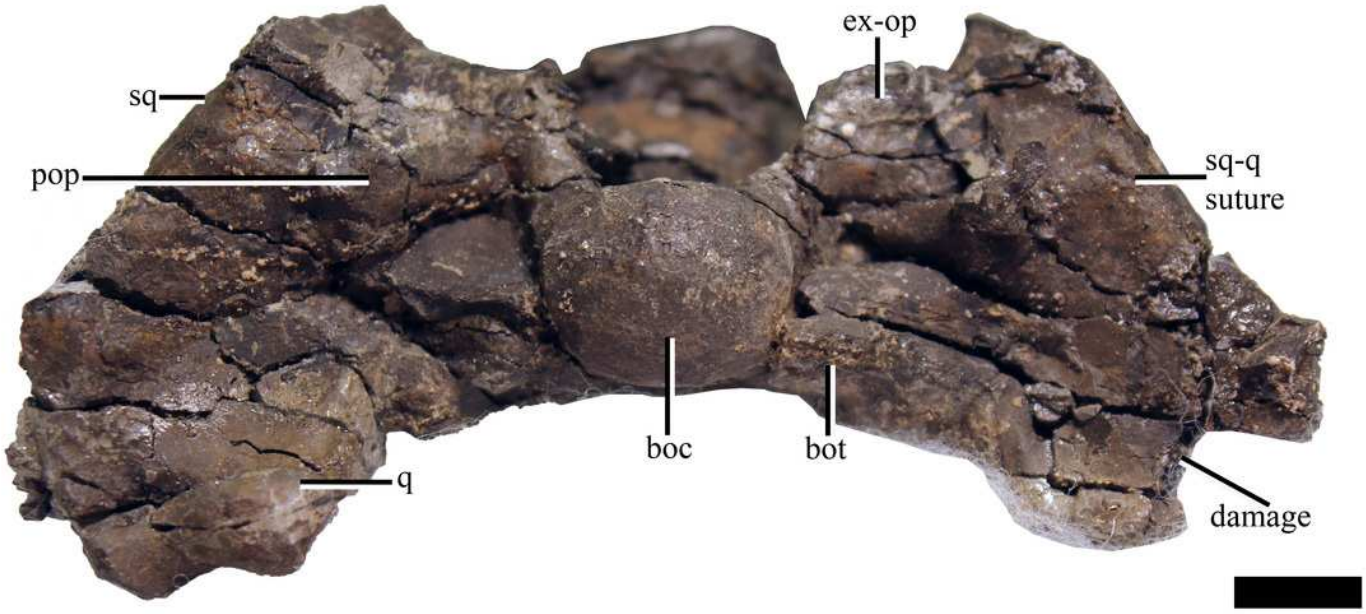

Figure 8

Surface reconstruction of the braincase and pterygoids of *Ophthalmothule cryostea,* PMO 224.248 using the µCT images.

In (A) dorsal, (B) anterodorsal and (C) lateral views. Abbreviations: aiv; anterior interpterygoid vacuity; ba, basal articulation; bo; basioccipital; boc, basioccipital condyle; bof, basioccipital foramina; bot, basioccipital tuber; dmp, dorsal median pit; ex-op; exoccipital-opisthotic; fo; fenestra ovalis; hsc, horizontal semicircular canal; pbs, parabasisphenoid; pitf, pituitary fossa; piv, posterior interpterygoid vacuity; pop, paraoccipital process; pro, prootic; pt, pterygoid; vsc, vertical semicircular canal. Scale bar equals 2 cm.

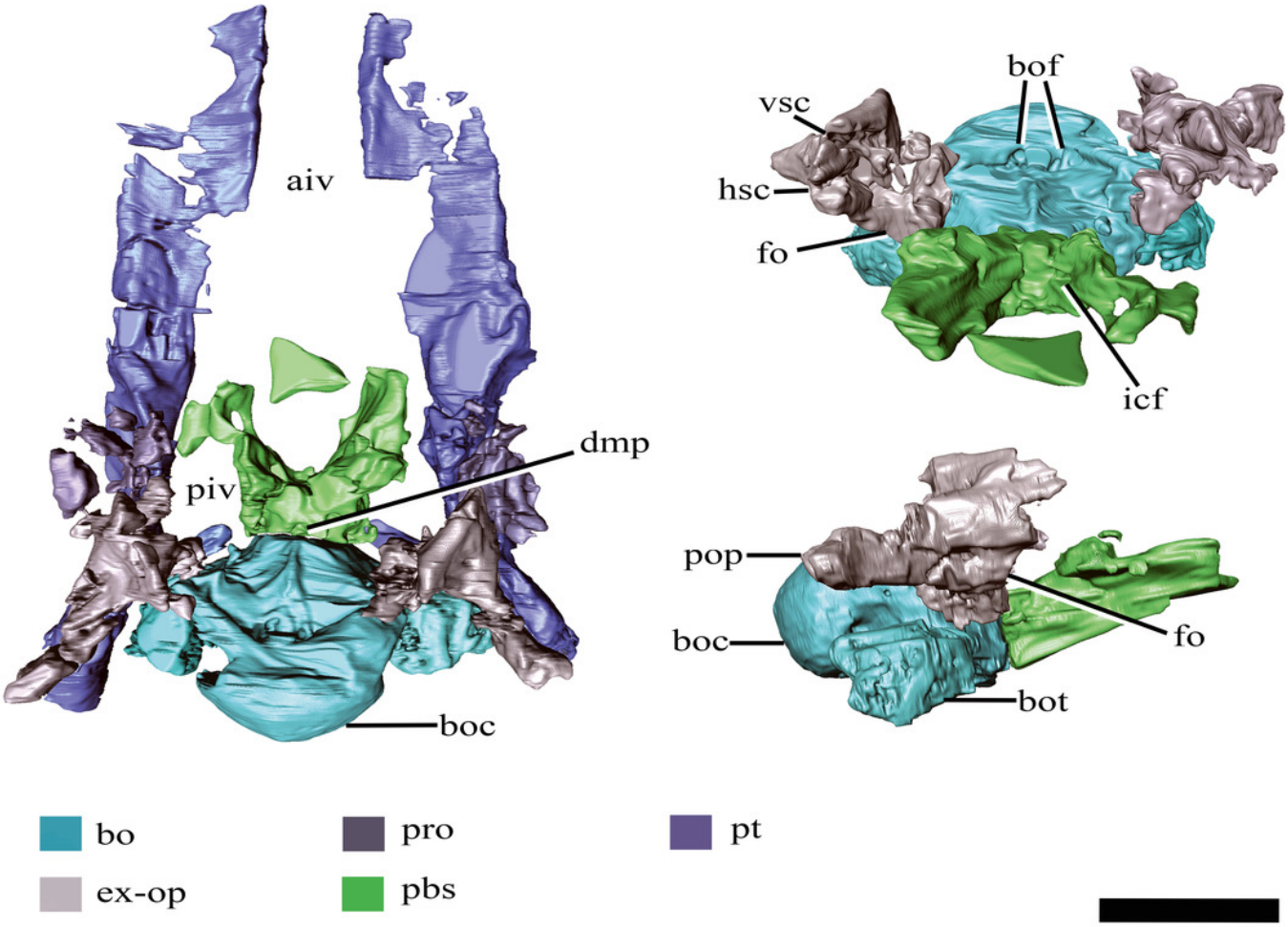
aiv
dmp
piv
boc
bof
vsc
hsc
fo
icf
pop
boc
fo
bot
bo
pro
pt
ex-op
pbs

Figure 9

The right exoccipital-opisthotic of *Ophthalmothule cryostea,* PMO 224.248 segmented out from µCT images.

In (A) posterior, (B) lateral, (C) anterior and (D) medial views. Abbreviations: bof, position of basioccipital facet; fo, position of fenestra ovalis; hsc, horizontal semicircular canal; pop, paraoccipital process; prof, position of prootic facet; sof, position of supraoccipital facet; sqf, position of squamosal facet; ut, utriculus; vsc, posterior vertical semicircular canal; X, position of cranial nerve openings. Scale bar equals ~1 cm

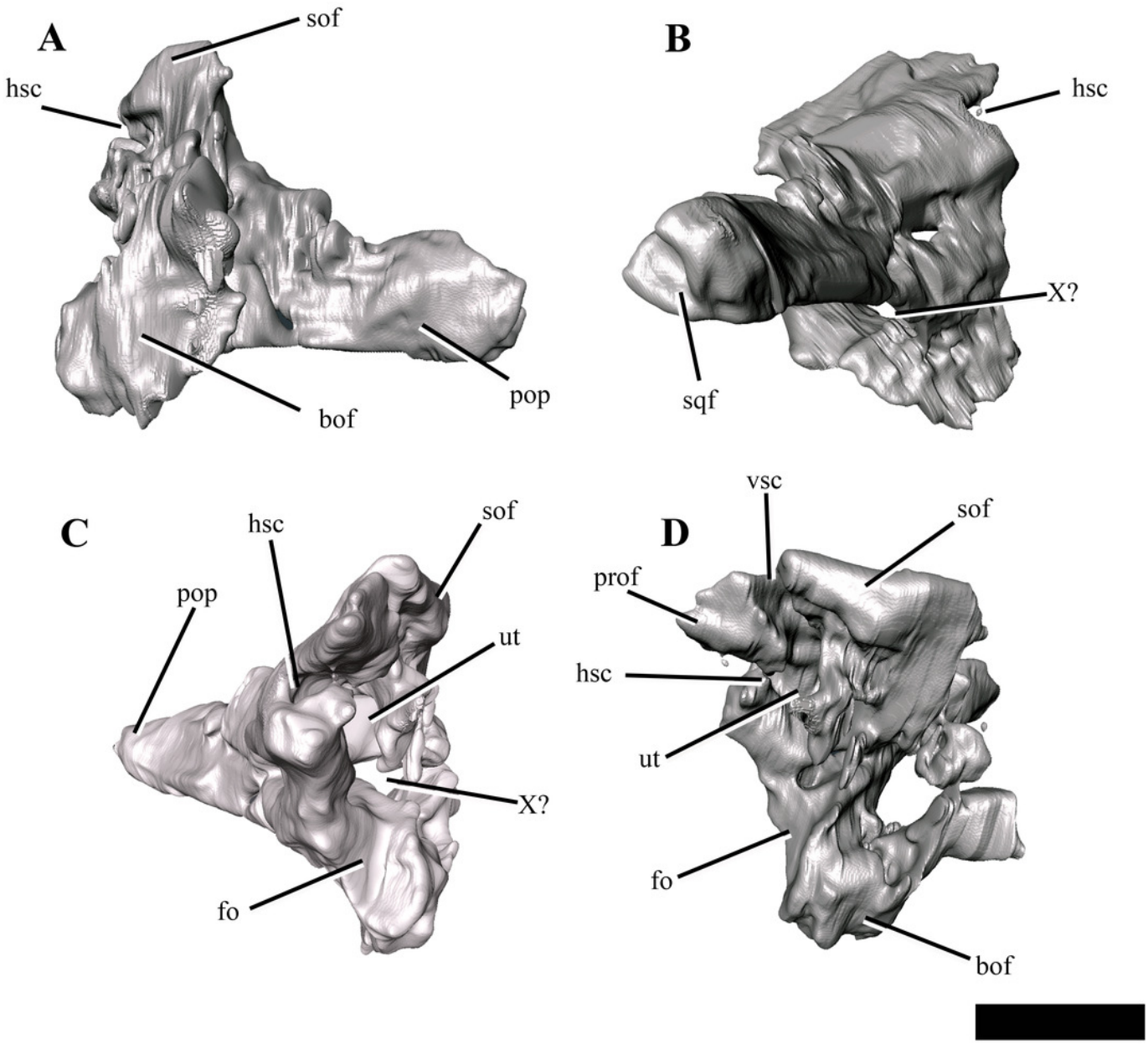
A
sof
hsc
pop
bof
B
hsc
X?
sqf
C
hsc
sof
pop
ut
X?
fo
D
vsc
sof
prof
hsc
ut
fo
bof

Figure 10

The left mandible of *Ophthalmothule cryostea,* PMO 224.248 shown as the computed tomography surface rendering and interpretations.

In (A-B) medial, (C-D) dorsal and (E-F) lateral views. Abbreviations: a, angular; alv, alveolus; art, articular; cp, coronoid process; d, dentary; sa, surangular; sp, splenial. Scale bar equals 2 cm.

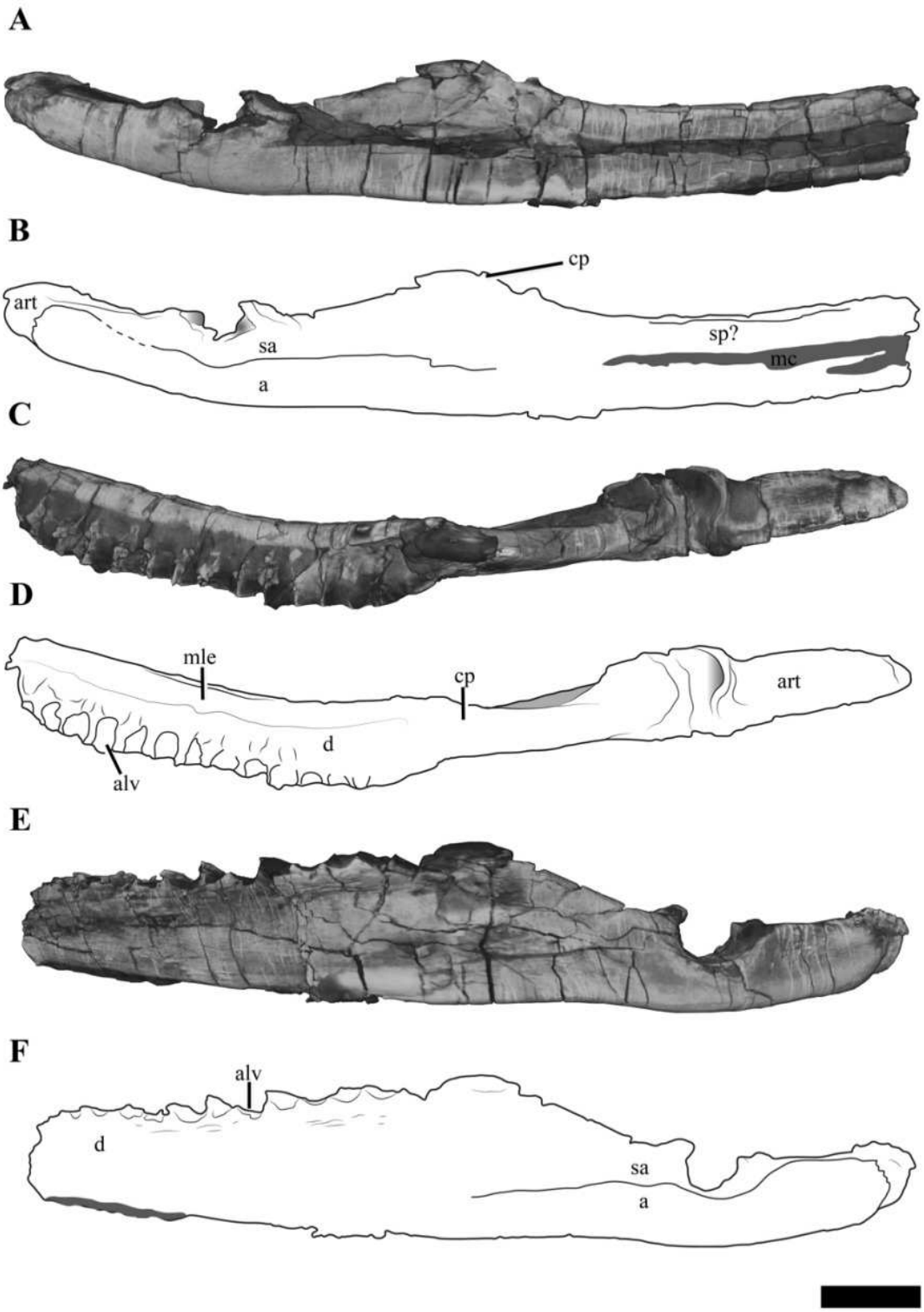
A
B
cp
art
sa
sp?
mc
a
C
D
mle
cp
art
d
alv
E
F
alv
d
sa
a

Figure 11

Isolated teeth of *Ophthalmothule cryostea,* PMO 224.248.

(A) the most complete tooth in axial view; (B-E) an incomplete tooth in (B,D) axial, (C), lingual and (E), labial views with a cross section of the tooth. Abbreviations: be, broken edge; rt, root tip. Scale bar equals 0.5 cm. Photography by Aubrey Roberts

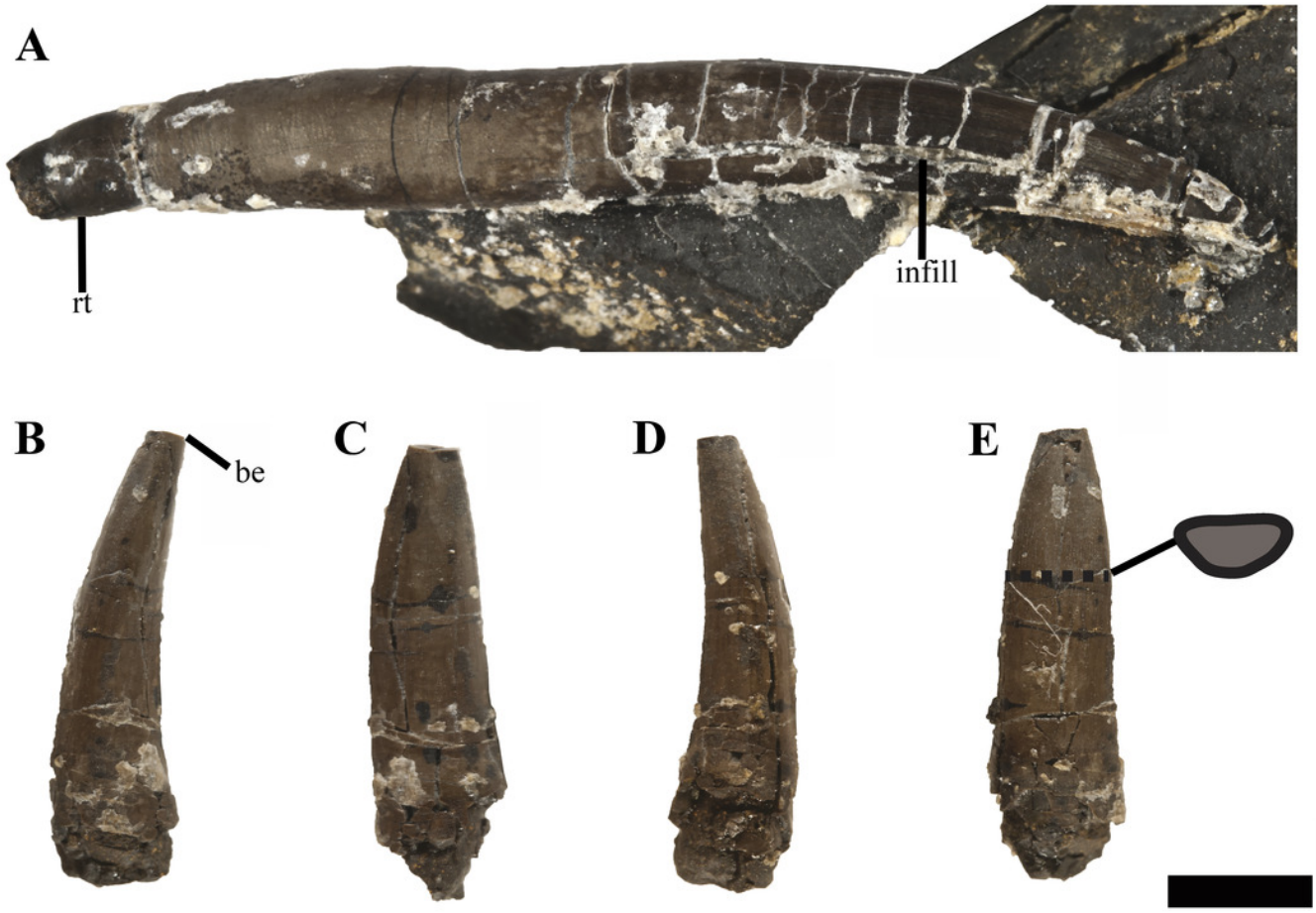

Figure 12(on next page)

Photos and interpretations of the atlas-axis complex of *Ophthalmothule cryostea,* PMO 224.268.

In (A-B) anterior, (C-D) lateral, (E-F) posterior and (G-H), ventral views. Abbreviations: aas, atlas-axis suture; atc, atlas centrum; atr, atlantal rib; axc, axial centrum; axr, axial rib; hyp, hypophyseal ridge; ns, neural spine; poz, postzygapophysis. Scale bar equals 1 cm. Photography by Aubrey Roberts

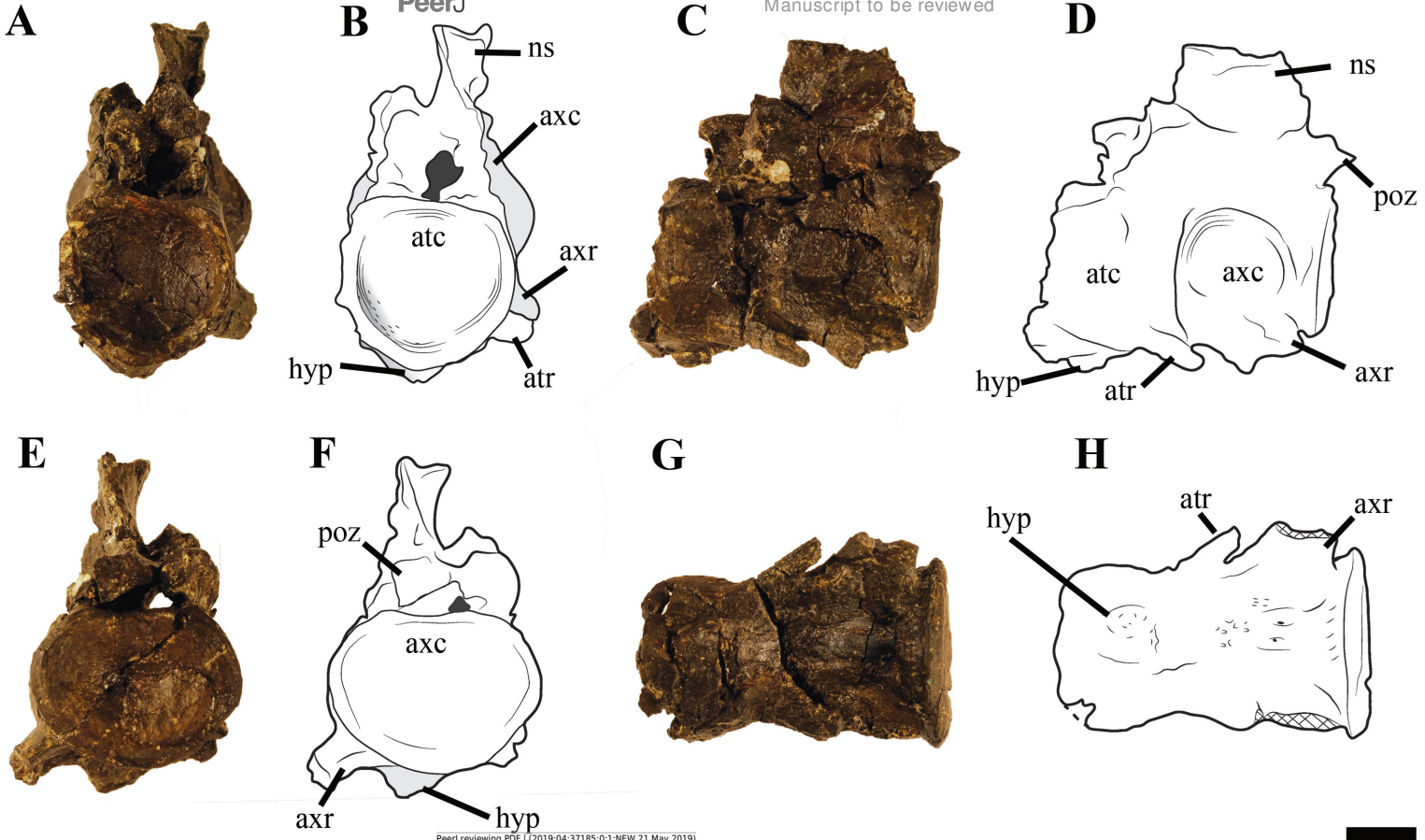
A
B
ns
axc
atc
axr
hyp
atr
C
D
ns
poz
atc
axc
hyp
atr
axr
E
F
poz
axc
axr
hyp
G
H
hyp
atr
axr

Figure 13

Selected anterior – mid cervical vertebrae of *Ophthalmothule cryostea,* PMO 224.248.

The 4th cervical vertebrae in (A) anterior, (B) lateral, (C) dorsal and (D) ventral views. (E) the 7th and 8th articulated cervical vertebrae in lateral view. (F) the articulated 14th and 15th cervical vertebrae in lateral view. (G) the 15th cervical in dorsal view. The 17th vertebrae in (H) anterior and (I) ventral views. Abbreviations: 3rd ns, neural spine from the 3rd cervical vertebrae; nc, neural canal; ns, neural spine; poz, postzygapophyses, prz, prezygapophyses, ri, ventral ridge; scf, subcentral foramina. Scale bar equals 2 cm. Photography by Aubrey Roberts

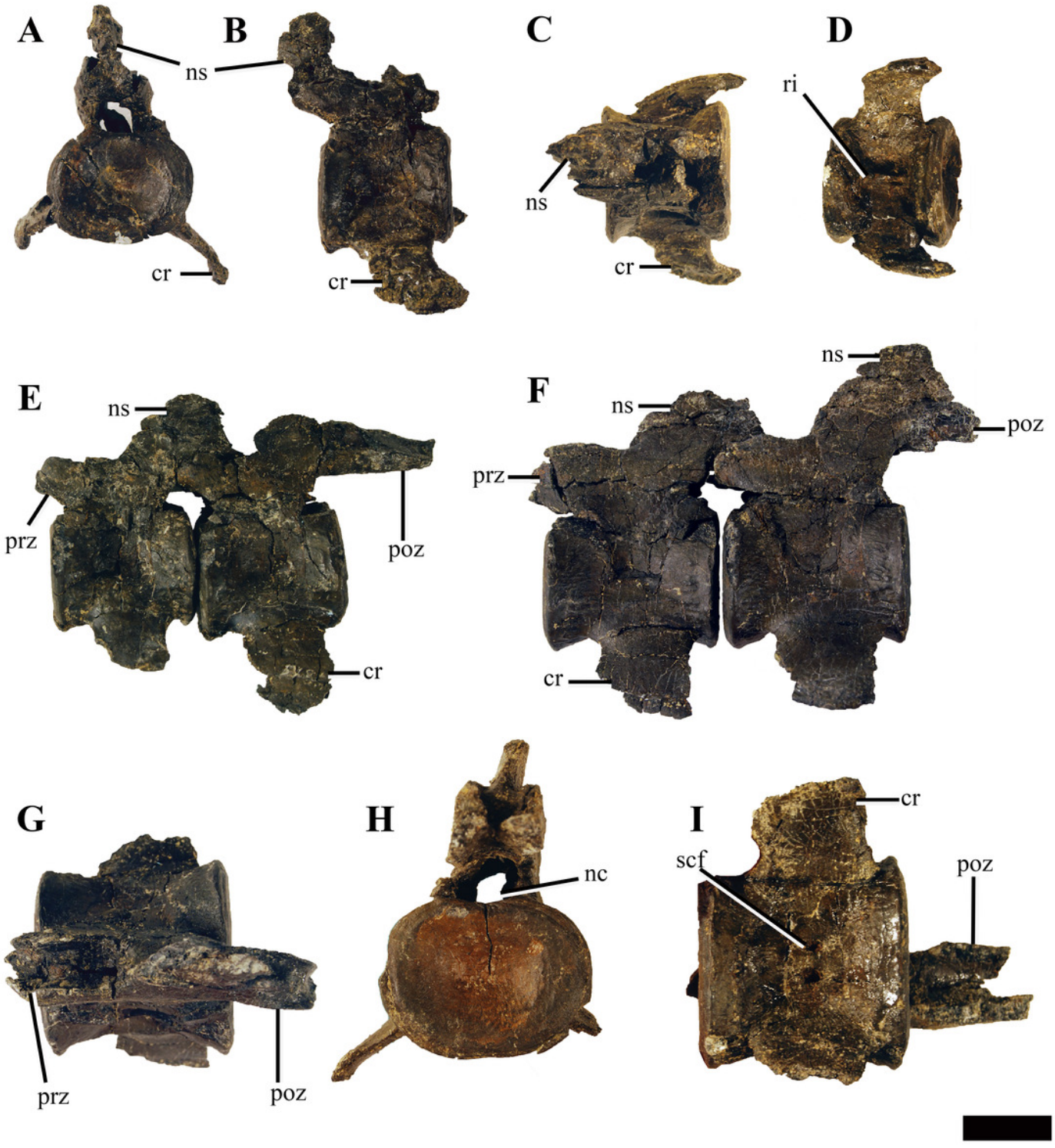
A
ns
cr
B
cr
C
ns
cr
D
ri
E
ns
prz
poz
cr
F
ns
ns
poz
prz
cr
G
prz
poz
H
nc
I
cr
scf
poz

Figure 14

Two posterior cervical vertebrae of *Ophthalmothule cryostea,* PMO 224.248.

The 29th cervical vertebra in (A) anterior, (B) posterior and (C) lateral views. The 44th cervical vertebra in (D) anterior, (E) dorsal and (F) ventral views. Abbreviations: cr, cervical rib; lrr, longitudinal rib ridge; nc, neural canal; nf, nutritive foramina; ns, neural spine; poz, postzygapophyses; prz, prezygapophyses; scf, subcentral foramina. Scale bar equals 4 cm. Photography by Aubrey Roberts

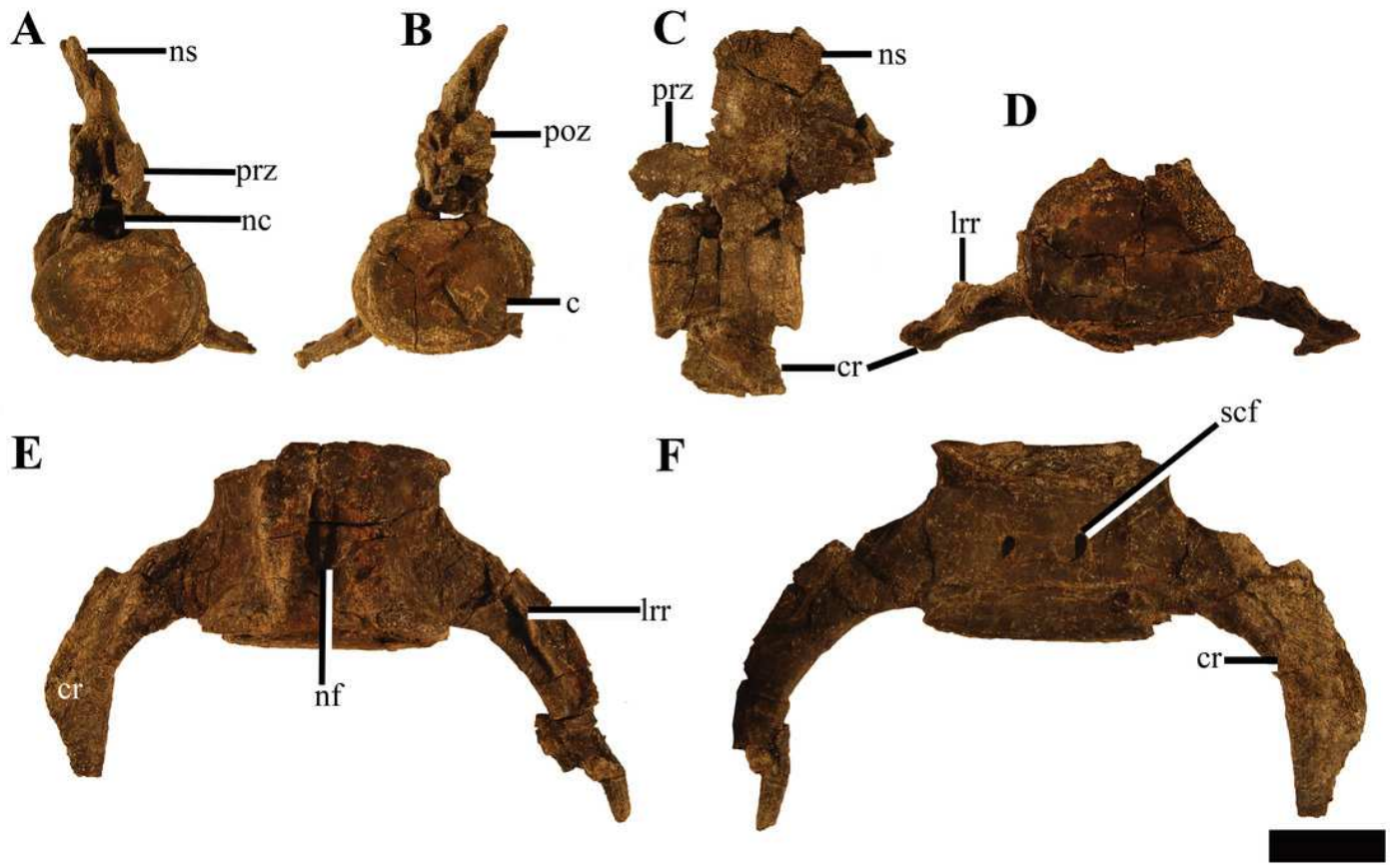

Figure 15

Pectoral vertebrae and pectoral ribs of *Ophthalmothule cryostea,* PMO 224.248.

The 1st pectoral in (A) anterior, (B) dorsal and (C) lateral views. The 2nd pectoral in (D) anterior, (E) ventral and (F) lateral views. (G), the 3rd pectoral vertebrae in posterior view. The 1st pectoral rib in (H) anterior, (I) posterior and (J) dorsal views. Abbreviations: fa, facet for the pectoral rib; lrr, longitudinal rib ridge; nf, nutritive foramina; rf, rib facet; scf, subcentral foramen. Scale equals 4 cm. Photography by Aubrey Roberts

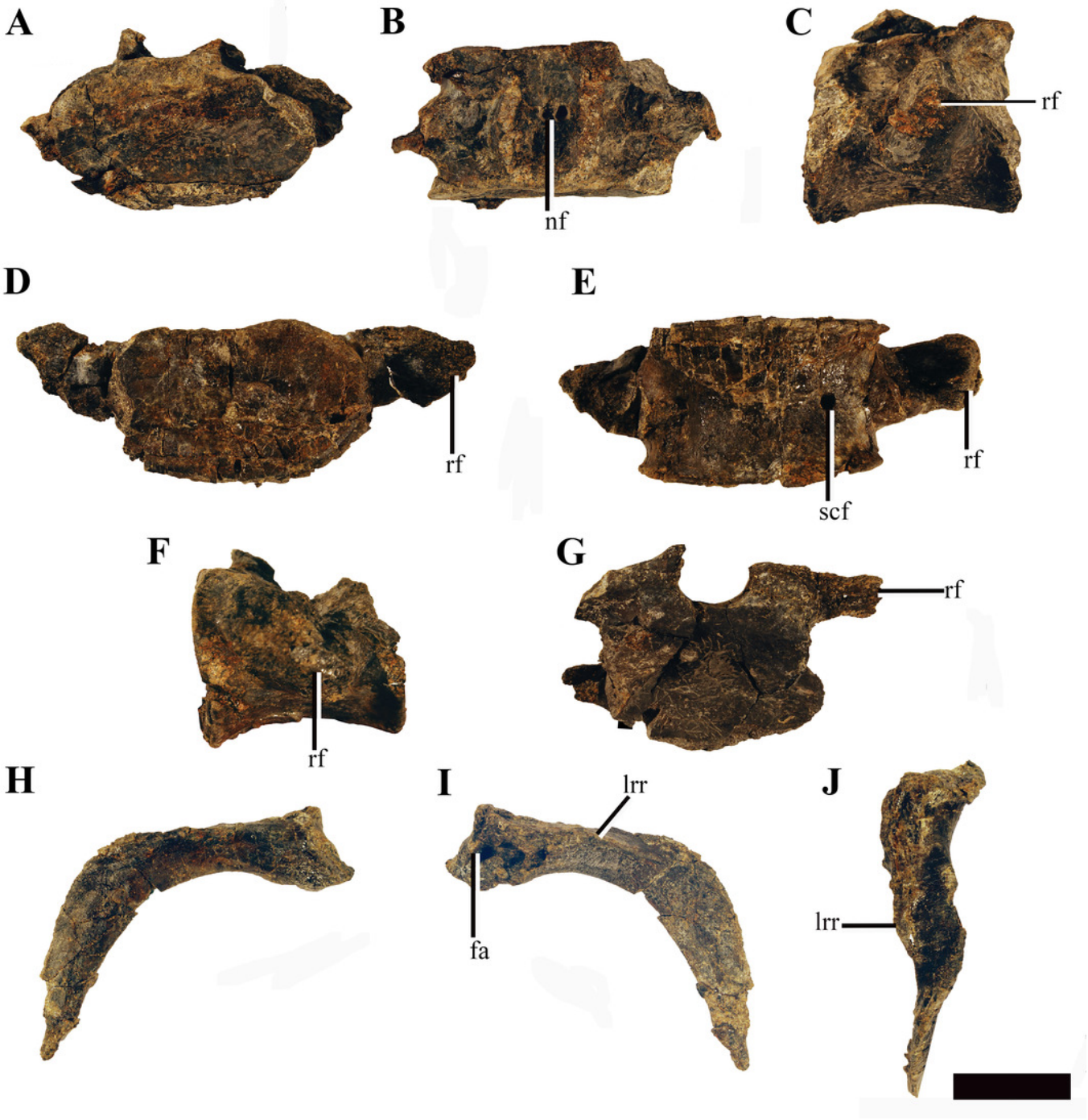
A
B
nf
C
rf
D
rf
E
rf
scf
F
rf
G
rf
H
I
lrr
fa
J
lrr

Figure 16

Dorsal vertebrae and ribs of *Ophthalmothule cryostea,* PMO 224.248.

The 1st dorsal vertebrae in (A) anterior and (B) ventral views. The 2nd dorsal vertebrae in (C) anterior, (D) lateral and (E) ventral views. The 3rd dorsal vertebrae in (F) anterior and (G) ventral views. Scale equals 2 cm. (H) a right anterior dorsal rib head in proximal view. (I) a complete rib in anterior view. Abbreviations: ph, proximal head; lrr, longitudinal rib ridge; scf, subcentral foramina; tp, transverse process. Scale equals 5 cm. Photography by Aubrey Roberts

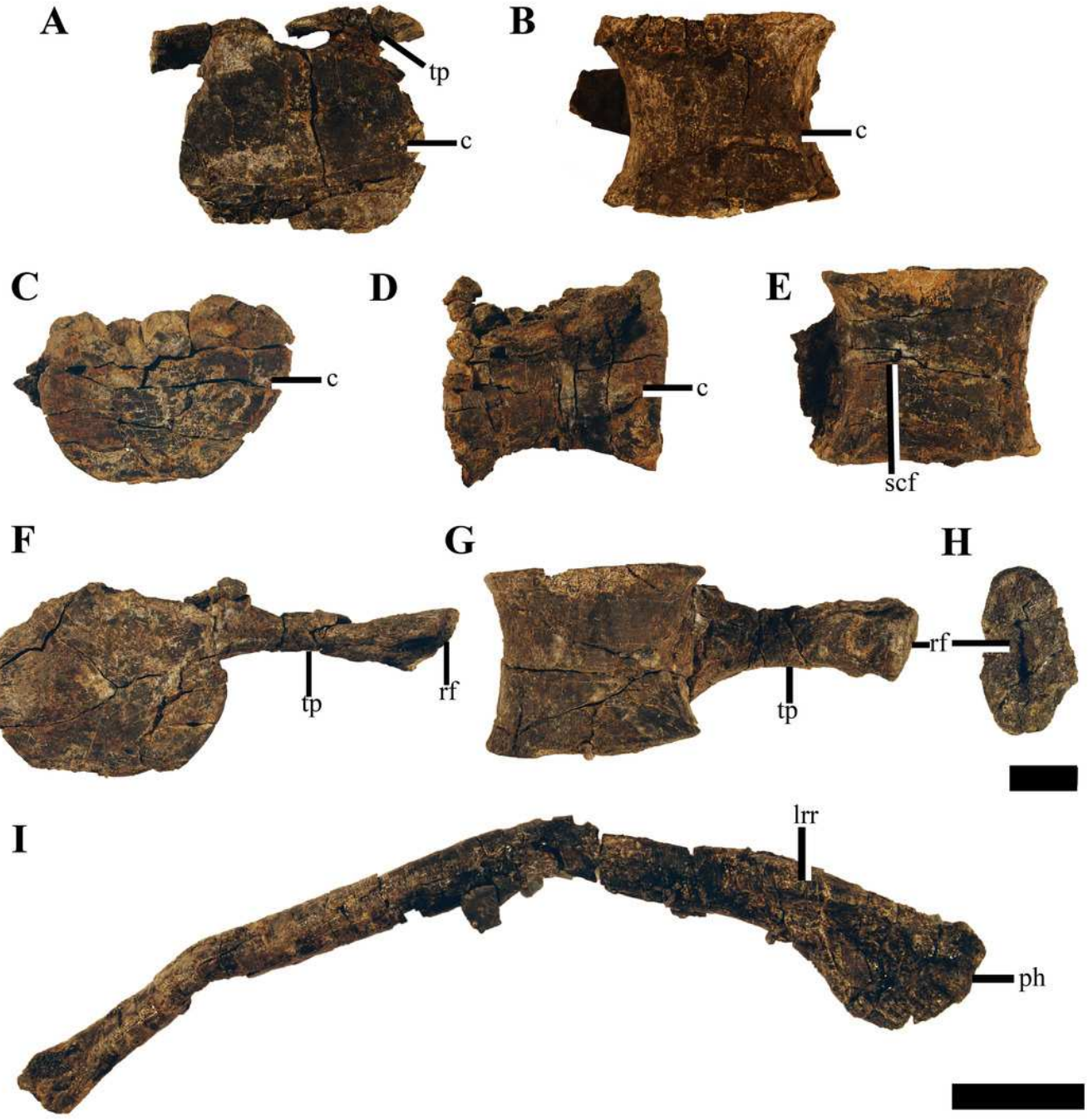
A
tp
c
B
c
C
c
D
c
E
scf
F
tp
rf
G
tp
H
rf
I
lrr
ph

Figure 17 (on next page)

The pectoral girdle of *Ophthalmothule cryostea,* PMO 224.248.

(A) the complete pectoral girdle, (B) interpretation and (C) reconstruction. Abbreviations: amp, anteromedial process of the coracoid; c, coracoid; cc, coracoid cornu; icl, interclavicle; pfn, pectoral fenestra; sc, scapula. Scale equals 5 cm. Photography by Aubrey Roberts

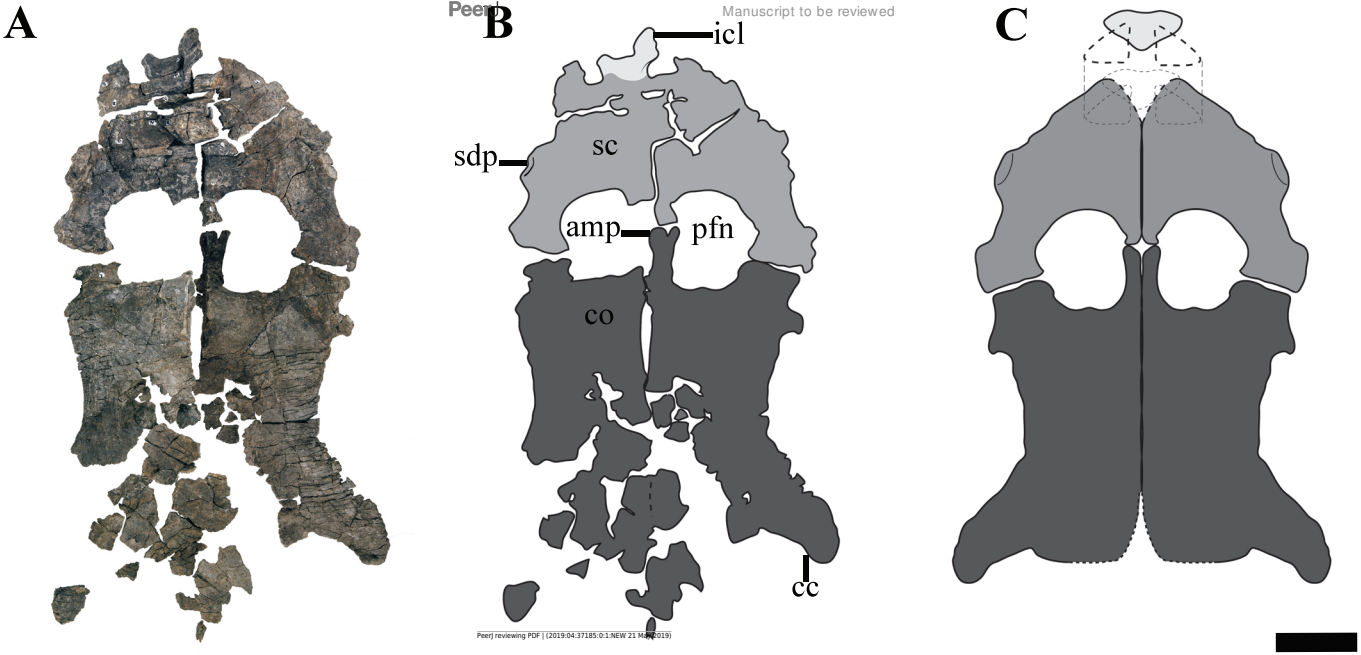

Figure 18

The left humerus and proximal limb elements of *Ophthalmothule cryostea,* PMO 224.248.

(A) the left forelimb with the proximal elements articulated in dorsal view. The left humerus in (B) ventral, (C) anterior, (D) proximal, (E) posterior and (F) distal views. Abbreviations; apf, additional postaxial facet; ca, capitilum; hu, humerus; i, intermedium; nf, nutritive foramina, paf, postaxial flange; pao, postaxial ossicle; praf, preaxial facet; r, radius; ra, radiale; rf, radius facet; ru, rugosity; u, ulna; uf, ulna facet; ul, ulnare. Scale bar equals 5 cm. Photography by Aubrey Roberts

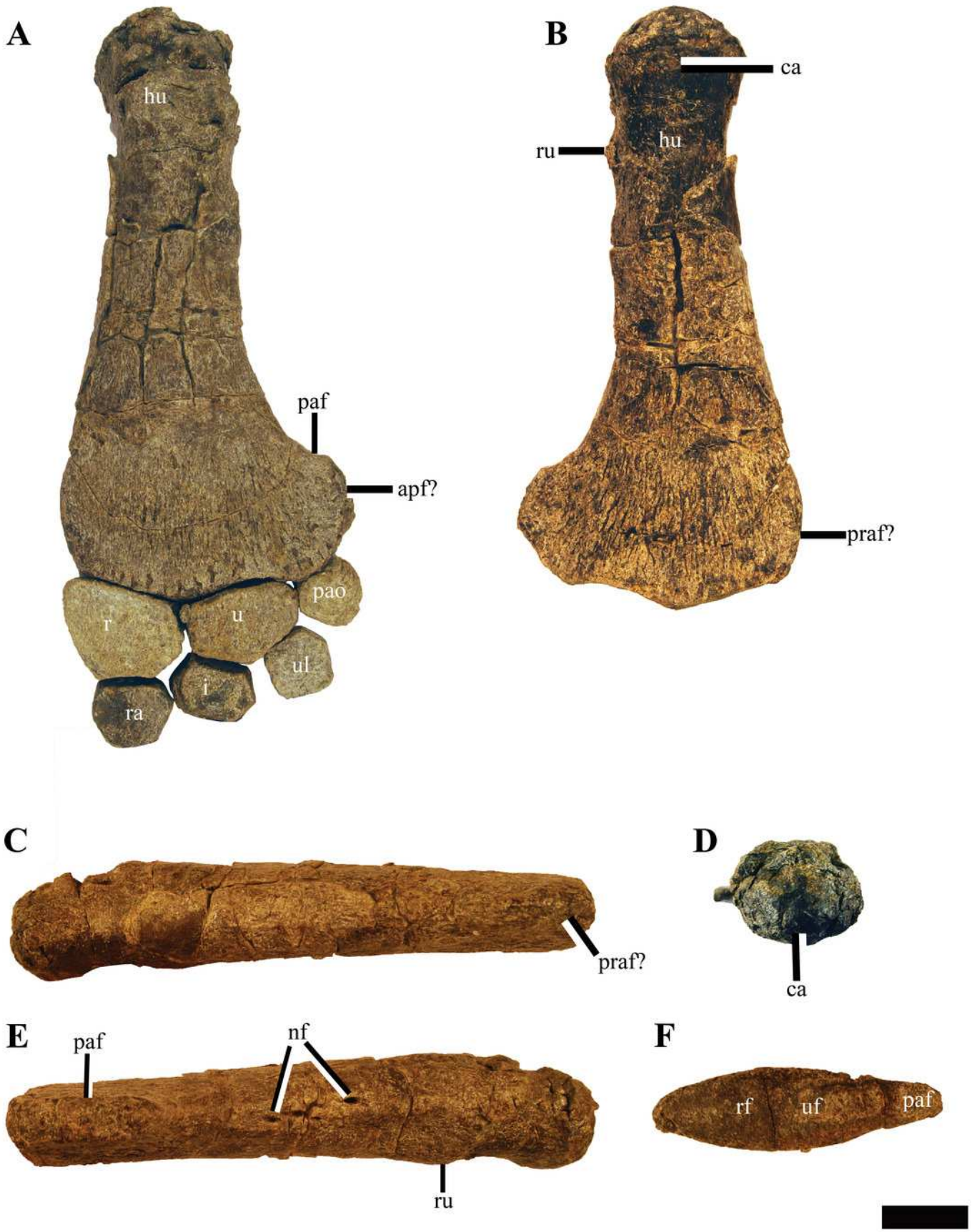
A
hu
paf
apf?
pao
r
u
ul
i
ra
B
ca
ru
hu
praf?
C
praf?
D
ca
E
paf
nf
ru
F
rf
uf
paf

Figure 19

Time scaled strict consensus tree of Plesiosauria with a focus on cryptoclidids.

Strict consensus tree of 144 MPTs with a tree length of 1321 (CI= 0.299 and RI = 0.663). Bremer support is shown below the clade branches. A more complete tree including Xenopsaria is available in ssupplementary information (Fig. S.14).

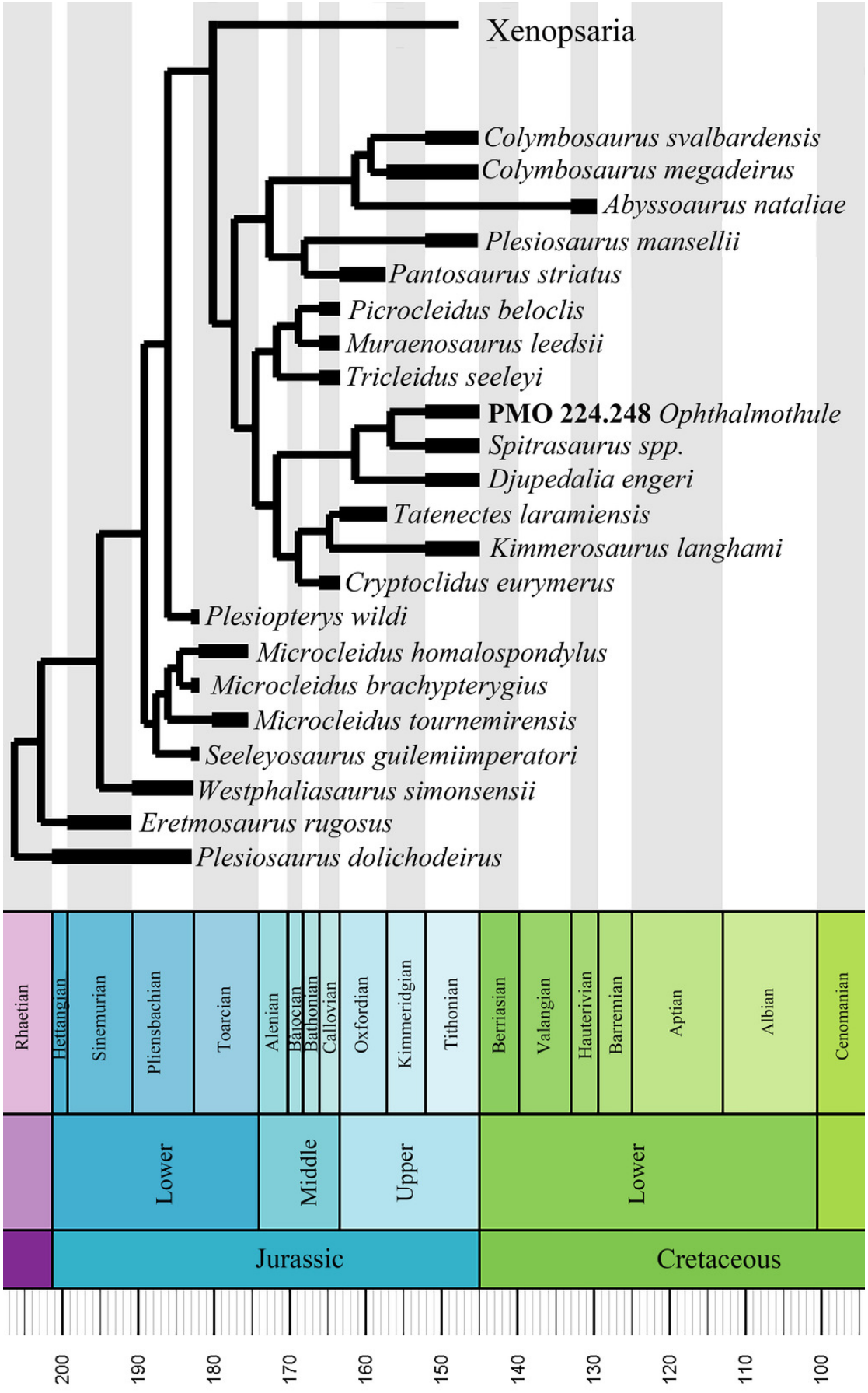
Xenopsaria
Colymbosaurus svalbardensis
Colymbosaurus megadeirus
Abyssoaurus nataliae
Plesiosaurus mansellii
Pantosaurus striatus
Picrocleidus beloclis
Muraenosaurus leedsii
Tricleidus seeleyi
PMO 224.248 Ophthalmothule
Spitrasaurus spp.
Djupedalia engeri
Tatenectes laramiensis
Kimmerosaurus langhami
Cryptoclidus eurymerus
Plesiopterys wildi
Microcleidus homalospondylus
Microcleidus brachypterygius
Microcleidus tournemirensis
Seeleyosaurus guilemiimperatori
Westphaliasaurus simonsensii
Eretmosaurus rugosus
Plesiosaurus dolichodeirus
Rhaetian
Hettangian
Sinemurian
Pliensbachian
Toarcian
Alenian
Bajocian
Bathonian
Callovian
Oxfordian
Kimmeridgian
Tithonian
Berriasian
Valangian
Hauterivian
Barremian
Aptian
Albian
Cenomanian
Lower
Middle
Upper
Lower
Jurassic
Cretaceous
200
190
180
170
160
150
140
130
120
110
100

Figure 20

A reconstruction of *Ophthalmothule cryostea* in its natural environment.

Illustration by Esther van Hulsen.